Gravity and Aeromagnetic Studies of the Santo Domingo Basin Area, New Mexico

By V.J.S. Grauch, David A. Sawyer, Scott A. Minor, Mark R. Hudson, and Ren A. Thompson

Chapter D of

The Cerrillos Uplift, the La Bajada Constriction, and Hydrogeologic Framework of the Santo Domingo Basin, Rio Grande Rift, New Mexico

Edited by Scott A. Minor

Professional Paper 1720–D

U.S. Department of the Interior
U.S. Geological Survey

Contents

Figures

Table

Gravity and Aeromagnetic Studies of the Santo Domingo Basin Area, New Mexico

By V.J.S. Grauch, David A. Sawyer, Scott A. Minor, Mark R. Hudson, and Ren A. Thompson

Abstract

Investigations of gravity and aeromagnetic data at both regional and local scales contribute to an overall understanding of the subsurface geologic and hydrogeologic framework of the Santo Domingo Basin area. Gravity data indicate that the Santo Domingo Basin is bounded on the southeastern side by steeply dipping faults of large vertical displacement and on the northwestern side by a homocline or series of down-to-basin faults. The Cerrillos uplift is reflected in a north-south gravity high that includes and is much larger than the area of Oligocene intrusions of the Ortiz Mountains and Cerrillos Hills, as indicated by the regional magnetic data. Within the La Bajada constriction, the gravity data and associated models indicate a northeast-trending trough 10–14-km wide that projects under the Cerros del Rio volcanic field; the trough likely contains Santa Fe Group sediments about 1 km thick. Moderate- to high-amplitude, positive aeromagnetic anomalies in the Cerros del Rio volcanic field are associated with basalts that formed during the Gauss normal magnetic-polarity epoch (2.70–2.59 Ma), whereas negative anomalies of similar amplitude are associated with basalts that formed during the Matuyama reversed magnetic-polarity epoch (2.59 Ma–776 ka). In the western half of the Cochiti Pueblo study area, magnetic piedmont basin-fill sediments of the Cochiti Formation and axial river gravels are expressed as subtle aeromagnetic anomalies that correlate with topography. Numerous faults that offset these magnetic sediments have aeromagnetic expressions that help delineate faults where they are concealed or inferred. An extensive northeast-elongated negative anomaly in the southern part of the intrabasin La Majada graben is interpreted as a post-2.59-Ma buried flow that dips to the east and ranges in depth from about 300 to 450 m. This interpretation implies that 525–725 m of displacement has occurred along the La Bajada fault zone during the last 2.4 m.y.

Introduction

Studies by the U.S. Geological Survey were begun in 1996 to improve understanding of the geologic framework of the Albuquerque composite basin and adjoining areas, in order that more accurate hydrogeologic parameters could be applied to new hydrologic models. The ultimate goal of this multidisciplinary effort has been to better quantify estimates of future water supplies for northern New Mexico's growing urban centers, which largely subsist on aquifers in the Rio Grande rift basin (Bartolino and Cole, 2002). From preexisting hydrologic models it became evident that hydrogeologic uncertainties were large in the Santo Domingo Basin area, immediately upgradient from the greater Albuquerque metropolitan area, and particularly in the northeast part of the basin referred to as the La Bajada constriction (see chapter A, this volume, for a geologic definition of this feature as used in this report). Accordingly, a priority for new geologic and geophysical investigations was to better determine the hydrogeologic framework of the La Bajada constriction area. This chapter along with the other chapters of this report present the results of such investigations conducted since 1996 by the U.S. Geological Survey.

Gravity and aeromagnetic methods are geophysical techniques that can be used to investigate the subsurface geology that influences groundwater flow and storage in the Santo Domingo Basin and adjoining parts of the Albuquerque and Española Basins. Gravity methods rely on measurements of the Earth's gravitational field at the surface to determine changes in bulk density of the crust, whereas aeromagnetic methods measure variations in the strength of the Earth's magnetic field from the air to determine variations in magnetization. From these measurements, geophysicists deduce the spatial distribution of the physical properties in the earth and interpret these distributions in terms of lithologic properties and subsurface structure.

Gravity studies can place constraints on basin geometry, the nature and orientation of basement structures, and regional variations in the thickness of basin fill. Aeromagnetic data help determine the lateral limits of intrusions, delineate buried faults and igneous rocks and, in some places, clearly distinguish between basalts extruded during different magnetic-polarity epochs. This chapter focuses on the methods and results of interpreting these kinds of features from gravity and aeromagnetic data at both regional scale for the Santo Domingo Basin and surrounding region (fig. A2) and at detailed scale for the Cochiti Pueblo area (fig. A4). We relied heavily on information and results from geophysical and geologic studies presented in other chapters of this

report. In the final chapter (chapter G), results from all studies described in this volume are brought together to construct a three-dimensional geologic framework and discuss its hydrogeologic implications. We first present background information on the data, methods, and types of approaches that we used to interpret the data. Next, we discuss regional interpretations from the gravity and aeromagnetic data, present a two-dimensional profile model that illustrates and integrates these interpretations, and discuss interpretations of high-resolution aeromagnetic data in more detail for the Cochiti Pueblo area. Finally, we summarize the salient results that were used to construct the three-dimensional geologic framework described in chapter G (this volume).

Gravity Data and Methods

Regional gravity studies have been critical in the definition of the basins and boundaries of the central Rio Grande rift from mid-1970s onward (Cordell, 1976, 1979; Birch, 1982; Ferguson and others, 1995; Grauch, Gillespie, and Keller, 1999). Gravity data are particularly effective in determining the subsurface configuration of basins within the Rio Grande rift, owing to the generally large contrast in density between the low-density basin fill (Santa Fe Group sediments) and the moderate- to high-density bedrock composing the basin floor and sides (pre-Miocene sedimentary and volcanic rocks and Precambrian basement). In addition, gravity data can be used to determine the location of basement uplifts and other major structures and the depths to which the Santa Fe Group sediments are linked between basins.

Data Compilation

Gravity data are typically collected in the field at individual stations and processed into Bouguer gravity anomaly data or Bouguer gravity data. These reductions include subtraction of theoretical or predicted values of the Earth's gravitational attraction at the elevation of the measurement point and removal of the effects of homogeneous masses underneath and adjacent to the measurement point (such as a neighboring hill). In this process, one must assume a certain density for the earth, typically 2,670 kg/m^3, so that the resulting variations shown on anomaly maps represent masses that deviate from that density.

In order to focus on density variations within the upper crust, a regional field is commonly removed from Bouguer gravity data. The regional field can be determined in a number of ways, such as trend fitting, modeling, or wavelength filtering. A regional field that is based on an Airy isostatic model is advantageous because it is understandable in physical terms and easily repeated between studies. Subtraction of the regional isostatic field from Bouguer gravity data gives isostatic residual gravity data, which can be used to examine density variations in the upper crust (Simpson and others, 1986). The exact parameters of the isostatic model need not be accurate nor does the Airy mechanism of isostasy need be completely satisfied for construction of a useful regional field (Simpson and others, 1986).

Isostatic residual gravity data for this study (pl. 3, fig. D1) were extracted from a recent compilation for the Albuquerque Basin area (Grauch, Gillespie, and Keller, 1999; Gillespie and others, 2000), which builds on data collected by previous workers since the 1970s. Data for the Santo Domingo Basin area originate primarily from the statewide compilation of Heywood (1992) and secondarily from a database of the Rio Grande rift maintained at the University of Texas at El Paso. In most of the Santo Domingo Basin area, the data provide adequate coverage (average station spacing of about 5 km, pl. 3) to represent regional gravity features (fig. D1).

Estimating Thickness of Basin Fill

The isostatic residual gravity map (pl. 3, fig. D1) primarily expresses variations in the thickness of the basin sediments. As a first-order approximation, lower values correspond with thicker fill. To estimate the thickness of basin fill from gravity data requires that one know the densities of sediments and rock units (or their average density differences) at various depths, measurements of thickness in many locations, or both. Because this information is limited in the Santo Domingo Basin region, we relied on a model developed as part of a study of the middle Rio Grande Basin (Grauch, Rodriguez, and Deszcz-Pan, 2002). This model covers a large region surrounding the Albuquerque Basin and includes the Santo Domingo and southern Española Basins.

In the regional model, basin-fill thickness was estimated by using an iterative three-dimensional modeling method that incorporates density versus depth functions for different geologic units (Jachens and Moring, 1990; Blakely and Jachens, 1991). Generalized density-depth functions for the modeling (fig. D2) were determined by use of density logs from wells in the Albuquerque Basin (Birch, 1982) and from a few additional wells located east of and outside the Santo Domingo Basin

Figure D1 (facing page). Isostatic residual gravity for the Santo Domingo Basin and surrounding areas, shown in color contours. Data extracted from Heywood (1992) and Gillespie and others (2000). Gray gradient lines that locate the steepest portions of gravity gradients were determined from regional horizontal-gradient magnitudes; line thickness corresponds with value of magnitude (see text). Thin magenta lines in the Cerrillos uplift outline aeromagnetic highs related to Eocene and Oligocene monzonite intrusions (pl. 4, fig. D5). Selected audiomagnetotelluric stations (chapter F, this volume) are represented by white triangles. Three deep wells near Valles caldera (PC–1, VC–1, AET–4) are discussed in the text. AE, Abiquiu embayment; CH, Cerrillos Hills; EA, El Alto graben of Cordell (1979); HB, Hagan bench; HEB, Hagan embayment; OM, Ortiz Mountains; SE, Santa Fe embayment; VG, Velarde graben of Cordell (1970); ZH, Ziana horst. Small black box outlines area of figure D7.

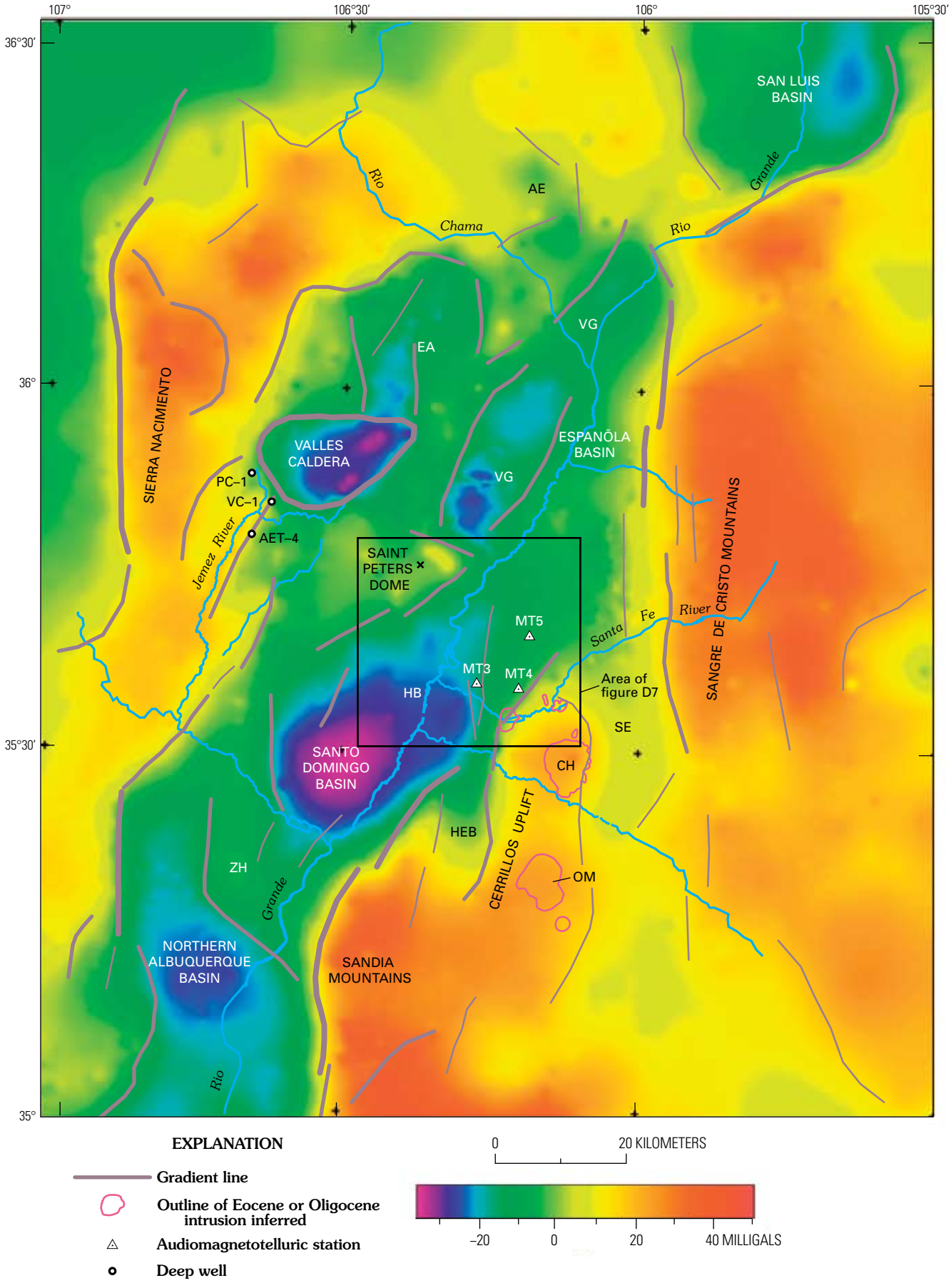
107°
106°30′
106°
105°30′
36°30′
36°
35°30′
35°
SAN LUIS BASIN
Rio Chama
Rio Grande
AE
VG
EA
SIERRA NACIMIENTO
VALLES CALDERA
ESPAÑOLA BASIN
PC–1
VC–1
AET–4
Jemez River
SAINT PETERS DOME
MT5
MT3
MT4
HB
Santa Fe River
SANGRE DE CRISTO MOUNTAINS
Area of figure D7
SE
SANTO DOMINGO BASIN
CH
HEB
CERRILLOS UPLIFT
OM
ZH
Rio Grande
NORTHERN ALBUQUERQUE BASIN
SANDIA MOUNTAINS
EXPLANATION
Gradient line
Outline of Eocene or Oligocene intrusion inferred
Audiomagnetotelluric station
Deep well
0
20 KILOMETERS
–20
0
20
40 MILLIGALS

(located on figs. D3, D4). We assumed that the Santa Fe Group is substantially less dense than older units at comparable depths (fig. D2), an assumption that generally allows the modeling procedure to separate the gravity effects of the Santa Fe Group from those of older units. Volcanic fields having great depth extent, such as the Jemez volcanic field, were given a separate density function (assumed to be 2,350 kg/m^3 on the basis of modeling of Nowell, 1996). Other volcanic areas consisting primarily of basalts no more than about 250 m thick, such as the Santa Ana and Cerros del Rio volcanic fields (SAMVF and CDRVF, fig. C1), were considered volumetrically unimportant compared with the mass of sediments contained in the basins (Cordell, 1976; Birch, 1982). As a consequence, the model represents the collective thickness of the volcanic units and the Santa Fe Group sediments in volcanic areas.

Because the model was constructed from limited information on thickness and density of sediments and rock units near the Santo Domingo Basin, the estimates of fill thickness should be viewed in a regional sense. If assumed densities are too high, estimated thicknesses will be too large; if assumed densities are too low, estimated thickness will be too small. For this report, we have subtracted the values of a subset of the regional thickness model (fig. D3) from smoothed topographic elevations to give an elevation model of the top of bedrock (fig. D4). The thickness model shows variations that may relate to potential aquifer thickness. The bedrock elevation model illustrates basin geometry.

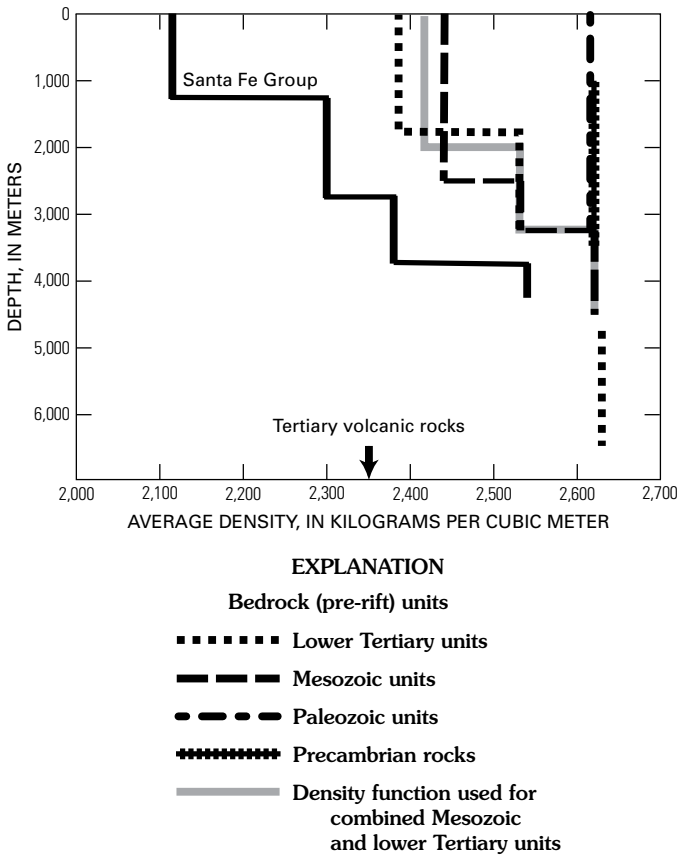

Figure D2. Density-depth step functions generalized from drill-hole density logs and used to construct the basin-fill thickness and bedrock elevation models (figs. D3 and D4, respectively). Densities of the high volume of Tertiary volcanic units in the vicinity of the Valles caldera could not be adequately characterized by drill-hole information. Instead, a constant density of 2,350 kg/m^3 was assumed (value marked by arrow at the bottom of the graph), on the basis of results of gravity modeling by Nowell (1996).

Locating Faults From Gravity Data

Steep gradients in the gravity field are commonly associated with abrupt lateral density contrasts, for example across faults or other steeply dipping surfaces such as homoclines. The horizontal-gradient method is commonly used to locate steep gradients, because the steepest parts of gradients are not necessarily obvious from inspection of gravity maps. Analogous to taking a derivative to find the inflection point of a curve, the method uses the local maxima of the magnitudes of the horizontal gradient to locate steep gradients (Cordell, 1979).

Gravity gradient lines (gray lines, fig. D1) mark the locations of steep gradients in the isostatic residual gravity field of the Santo Domingo Basin area. These lines were derived by using a modification to the horizontal-gradient method that focuses on regional gradients (Grauch and Johnston, 2002) and are generally similar to those computed by Cordell (1979) north of lat 35°30′N. These gradients are likely associated with major faults or homoclines. The gradients having the greatest magnitude, represented by the thickest lines (fig. D1), indicate that materials with contrasting densities are juxtaposed at steeply dipping faults (or fault systems) that extend to considerable depth, implying large throw on the fault (or faults). The gradients having the smallest magnitudes, represented by thin lines, indicate either smaller throw, less contrast in density, or structures that dip more shallowly, such as multiple, small, synthetic faults or a homocline. The locations of the lines may be shifted down-dip over nonvertical structures (Grauch and Cordell, 1987).

Figure D3 (facing page). Contours of estimated thickness of upper Cenozoic basin fill in Santo Domingo Basin area derived from a gravity model covering a much larger area (Grauch, Rodriguez, and Deszcz-Pan, 2002). Basin fill composed primarily of Santa Fe Group sediments, but it also contains basalts erupted from the Cerros del Rio (CDRVF) and Santa Ana Mesa (SAMVF) volcanic fields (figs. A2, C1). The model should be used only to define general geometry, owing to limitations of density assumptions, regional data coverage, and lack of deep drill-hole constraints in the Santa Domingo Basin area. Wells used to constrain the model are shown. Magnetotelluric stations described in chapter F (this volume). HEB, Hagan embayment; NAB, northern Albuquerque Basin. The geophysical model shown in figure D6 located along line of cross section, which is coincident with geologic cross section F-F′ (pl. 6F) or F-F″ (chapter G, this volume).

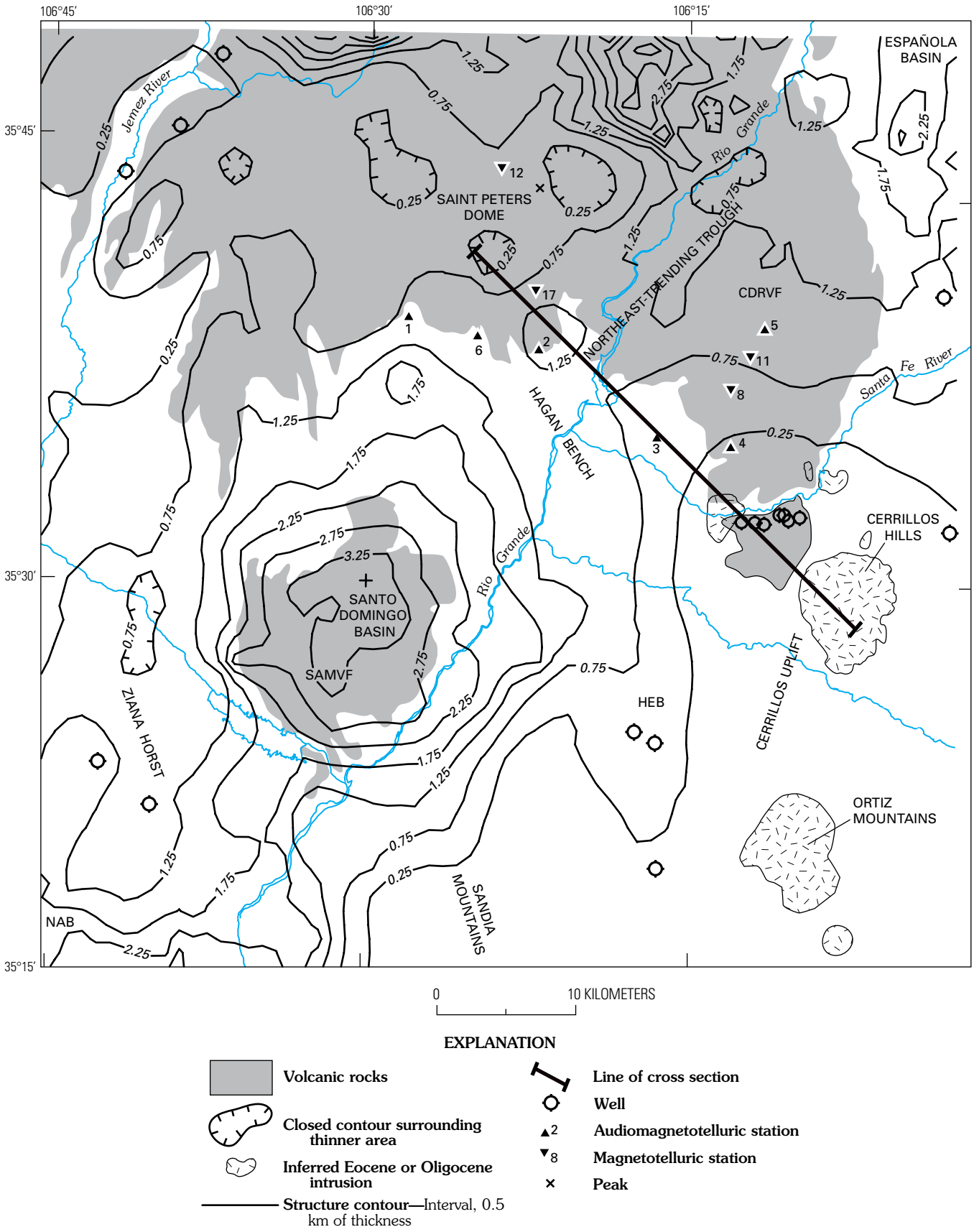
106°45′
106°30′
106°15′
35°45′
35°30′
35°15′
ESPAÑOLA BASIN
Jemez River
Rio Grande
Santa Fe River
SAINT PETERS DOME
NORTHEAST-TRENDING TROUGH
CDRVF
HAGAN BENCH
CERRILLOS HILLS
SANTO DOMINGO BASIN
SAMVF
ZIANA HORST
HEB
CERRILLOS UPLIFT
ORTIZ MOUNTAINS
SANDIA MOUNTAINS
NAB
0.25
0.75
1.25
1.75
2.25
2.75
3.25
1
2
3
4
5
6
8
11
12
17
0
10 KILOMETERS
EXPLANATION
Volcanic rocks
Closed contour surrounding thinner area
Inferred Eocene or Oligocene intrusion
Structure contour—Interval, 0.5 km of thickness
Line of cross section
Well
▲2 Audiomagnetotelluric station
▼8 Magnetotelluric station
× Peak

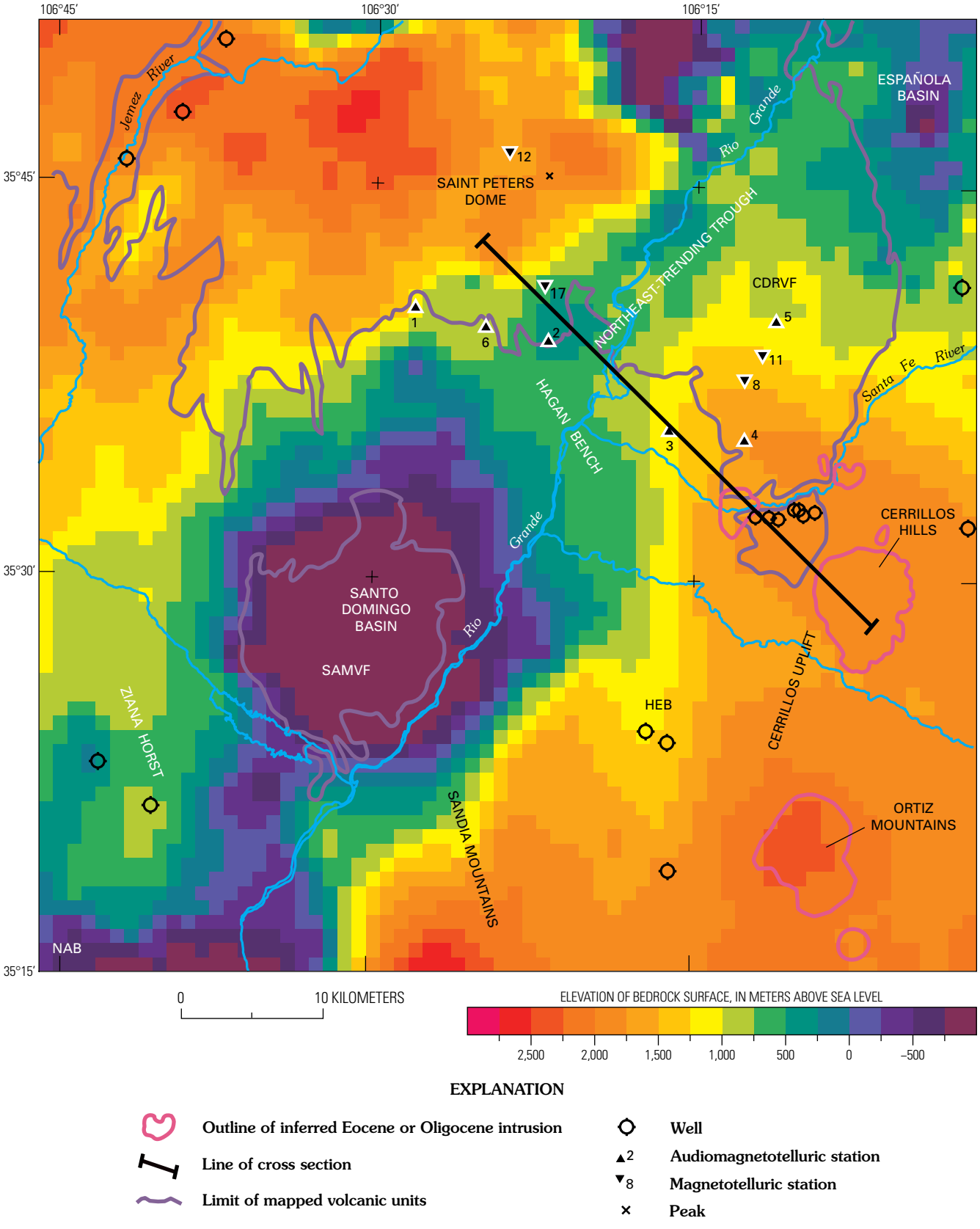

EXPLANATION

- Outline of inferred Eocene or Oligocene intrusion
- Line of cross section
- Limit of mapped volcanic units
- Well
- ▲2 Audiomagnetotelluric station
- ▼8 Magnetotelluric station
- × Peak

Figure D4 (facing page). Estimated elevation of bedrock at base of upper Cenozoic basin fill in the Santo Domingo Basin area; map provides general guides for basin geometry. Bedrock elevation model was constructed by subtracting values of the thickness model (fig. D3) from corresponding values of a digital elevation model that was first smoothed by use of a running- average technique. CDRVF, Cerro del Rio volcanic field; HEB, Hagan embayment; NAB, northern Albuquerque Basin; SAMVF, Santa Ana Mesa volcanic field. The geophysical model shown in figure D6 located along line of cross section, which is coincident with geologic cross section F-F′ (pl. 6*F*) or F-F″ (chapter G, this volume).

An example of the advantages of the horizontal-gradient method is shown by the gradient that surrounds the gravity low associated with the Valles caldera (fig. D1). The gradient varies in steepness around the gravity low, so the steepest part (gradient line) is not necessarily obvious from the color contours. Another example is at the northern tip of the Sandia Mountains (fig. D1), where the gradient line is oriented more southerly than the obvious trend of the color contours, creating an en echelon configuration with the gradient line to the south.

Aeromagnetic Data and Methods

Aeromagnetic methods traditionally have been used to map solely crystalline basement and igneous rocks at depth. Recent work in the Albuquerque Basin has demonstrated that these methods are also useful for mapping faults that offset basin fill and for delineating buried igneous bodies in the near surface (Grauch, 2001a). Aeromagnetic data represent variations in the strength of the Earth's magnetic field that are produced by changes in magnetization of the crust. Magnetization of rocks is determined by the quantity of magnetic minerals (commonly titanomagnetites) and by the strength and direction of remanent magnetization carried by those magnetic minerals. The quantity of magnetic minerals is measured as magnetic susceptibility and produces an induced magnetization. The remanent magnetization is based on the permanent alignment of magnetic domains within the rock and is measured using paleomagnetic methods (Butler, 1992; chapter C, this volume).

Aeromagnetic surveys respond to the total magnetization of rocks, which is the vector sum of the induced and remanent magnetizations. Igneous and crystalline metamorphic rocks commonly have high total magnetizations compared with other rock types, whereas sedimentary rocks and poorly consolidated sediments have much lower magnetizations (Reynolds and others, 1990; Hudson and others, 1999). The induced component is dominant in Santa Fe Group units, although total magnetization is fairly low. Moreover, higher magnetic susceptibilities generally correspond with coarser grained units (Hudson and others, 1999). In contrast, the remanent component is commonly dominant in volcanic units, which have high total magnetizations (Bath, 1968; Reynolds and others, 1990). Volcanic rocks with reverse-polarity remanent components that dominate total magnetization produce distinctive, high-amplitude negative aeromagnetic anomalies, such as the ones corresponding with the basalt at Santa Ana Mesa (fig. D5). Strong, positive aeromagnetic anomalies related to volcanic units can be inferred to indicate a normal-polarity magnetization, although these anomalies may be caused by dominant induced components as well.

Data Compilation

The aeromagnetic data for this study were assembled from a regional data compilation and two detailed airborne geophysical surveys: the Cochiti survey, generally flown over Cochiti Pueblo lands, and the Sandoval–Santa Fe survey, which covers the rest of the study area and overlaps with the Cochiti survey (U.S. Geological Survey, Sander Geophysics, Ltd., and Geoterrex-Dighem, 1999). The Cochiti survey, which was designed primarily to collect electromagnetic data (chapter F, this volume), was flown with 400-m line spacing; the magnetometer was nominally 73 m above ground. The Sandoval–Santa Fe survey, which was designed to gather high-resolution magnetic information, was flown with 150-m line spacing; the magnetometer was nominally 150 m above ground. Data from the surveys were analytically continued to a common observation surface 100 m above ground, digitally merged onto a grid with 50-m intervals, and then transformed by a standard reduction-to-pole operation (Sweeney, Grauch, and Phillips, 2002). This last operation, resulting in reduced-to-pole (RTP) data (Blakely, 1995), corrects for shifts of the main anomaly from the center of the magnetic source that occur at most latitudes owing to the oblique orientation of the measured magnetic field with respect to the Earth's surface (the field is vertical only at the magnetic poles). A similar operation, called the pseudogravity transformation or computation of the magnetic potential (Blakely, 1995), also minimizes these shifts, but at the same time considerably reduces the resolution of the data. This operation is commonly an interim step in methods that locate faults or estimate source depths (discussed below). The RTP and pseudogravity transformations require an assumption about the directions of magnetization of the magnetic sources. Generally, it is assumed that the total magnetizations of most rocks in the study area align parallel or anti-parallel to the Earth's main field (in the study area, declination is 11°, inclination is 63°). This collinearity assumption probably works well in most of the survey area, because the primarily Tertiary rock units have been rotated large amounts only in isolated areas (chapter E, this volume).

The final aeromagnetic compilation is displayed in color shaded relief (color plus illumination) on plate 4 and figure D5. The colors primarily reflect the broad variations in the data, whereas the illumination emphasizes detailed variations, especially those that are somewhat linear. The regional data were extracted from a state compilation in which the data were

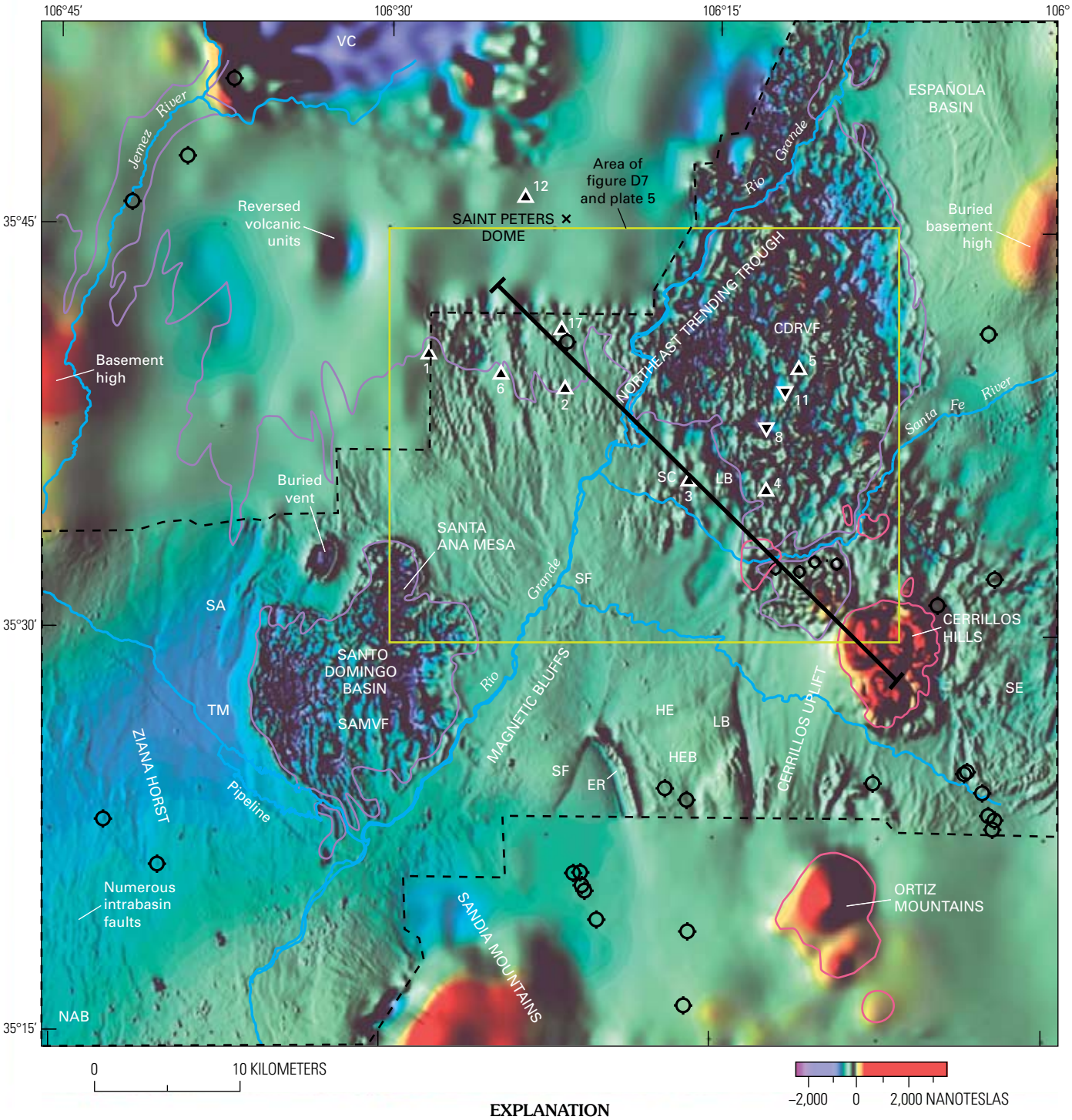

EXPLANATION

- Outline of inferred Eocene or Oligocene intrusion
- Line of cross section
- Limit of mapped volcanic units
- Limit of detailed aeromagnetic surveys
- Well
- ▲2 Audiomagnetotelluric station
- ▼8 Magnetotelluric station
- × Peak

Figure D5 (facing page). Reduced-to-pole aeromagnetic data for the Santo Domingo Basin area shown in color shaded relief, illuminated from the west. Detailed data combined with regional data are from Sweeney, Grauch, and Phillips (2002). Outlines of Oligocene intrusions determined from aeromagnetic data. CDRVF, Cerro del Rio volcanic field; ER, Espinaso Ridge; HE, Hagan Embayment fault zone; HEB, Hagan embayment; LB, La Bajada fault zone; NAB, northern Albuquerque Basin; SA, Santa Ana fault; SAMVF, Santa Ana Mesa volcanic field; SC, Sanchez fault; SE, Santa Fe embayment; SF, San Francisco fault; TM, Tamaya fault; VC, Valles caldera. The geophysical model of figure D6 is located along the line of cross section.

continued to a surface 300 m above ground (Kucks, Hill, and Heywood, 2001). The lower resolution of the Cochiti survey compared with the Santa Fe–Sandoval survey is evident by the discontinuous appearance of linear anomalies, such as those surrounding magnetotelluric station 17 near the northern boundary of the survey (pl. 4, fig. D5), which is caused by inadequate information between flight lines.

Locating Faults From Aeromagnetic Data

High-resolution aeromagnetic data allow discrimination of many subtle linear to arcuate features in areas where magnetic relief is fairly low (pl. 4, fig. D5); these features are enhanced by shading in the image display. These linear to arcuate patterns commonly correspond with geologically mapped faults and are produced by the juxtaposition of variably magnetic sediments (Grauch, Hudson, and Minor, 2001). The aeromagnetic expression of known faults can then be used to extend faults beyond their mapped surface exposure or to infer previously unknown faults where they are covered by thin surficial deposits (Grauch, 2001b).

Analogous to its use with gravity data, the horizontal-gradient method can be applied to RTP aeromagnetic or pseudogravity data to derive gradient lines that locate steep gradients associated with faults (Cordell and Grauch, 1985; Grauch, Hudson, and Minor, 2001). However, interpretation of the gradients is more ambiguous because of the high resolution of the aeromagnetic data, the effects of magnetic terrain (Grauch and Cordell, 1987), and the greater variability of magnetic properties compared with those of density. The locations of maxima from the horizontal-gradient method (using RTP data or pseudogravity data) can represent the locations of (1) faults, where a magnetic contrast is produced by structural juxtaposition of units; (2) contacts, where the magnetic contrast is produced by the limit of deposition of a magnetic unit against a less magnetic one; (3) steep topographic slopes, where the magnetic contrast is produced by the interface between rock and air; or (4) abrupt changes in magnetization within one rock unit, produced by primary differences in magnetization or by secondary destruction or growth of magnetic minerals. In addition, multiple gradients can occur where thin, horizontal sheet-like sources are vertically offset from thicker sources at depth, a distribution of rock units called a thin-thick layers model (Grauch, Hudson, and Minor, 2001).

Faults were interpreted for the Cochiti Pueblo area (pl. 2) from RTP magnetic data and maps of the horizontal-gradient magnitude of RTP magnetic data and pseudogravity (not shown), based on the following criteria. First, only linear or extensive semilinear gradients were considered; this criterion eliminates gradients produced by abrupt changes in magnetization within one rock unit. Second, gradients judged as due solely to topographic slopes were eliminated. Finally, multiple gradients were inspected in relation to topography and geology to determine if they were produced by a fault that fits the thin-thick layers model or by multiple faults. High-magnitude gradients corresponding with moderate to low topographic relief indicate that a magnetization contrast in addition to the topographic slope must be present. These gradients were interpreted as faults because topography commonly correlates with faults. High-magnitude gradients at high-relief topographic slopes required geologic examination to determine if the slope was caused by an erosional edge, a contact, or a fault. A particular origin could not be definitively determined for many gradients, so that many of them are not shown on the geologic map (pl. 2).

Estimating Depth

Depths to the tops of rock bodies were estimated from aeromagnetic data for the Cochiti Pueblo area in two ways—one based on horizontal gradients that operates on the entire grid of data and one that applies multiple algorithms along a profile of data in order to determine a consensus of solutions pertaining to individual anomalies. The method based on horizontal gradients uses the premise that anomalies with broad gradients are produced by deeper sources than those with steep gradients (Blakely, 1995). By measuring the width of the horizontal gradient curve, an estimated depth to the source can be computed (Roest and Pilkington, 1993; Phillips, 1997). Phillips (2000) determined that depth estimates are accurate for contacts that extend to great depth where the method is applied to RTP data and for contacts that extend only to shallower depths (such as those of a sheet) where the method is applied to pseudogravity data. Because the depths to which the contacts extend are unknown, solutions from RTP and pseudogravity data can be viewed as minimum and maximum estimates of the true depth (Phillips, 2000). The advantage of this method is its comprehensive coverage of the area and its ability to examine gradients that have various orientations. Its disadvantage is the dependence on the shape of the source body and problems with interference from neighboring sources (Phillips, 2000). Selected depth estimates derived from the RTP and pseudogravity data for the Cochiti Pueblo area are shown on plate 5.

The approach using profile data applies multiple depth-estimation algorithms (computer program PDEPTH; Phillips, 1997) to compute many depth solutions (locations

in three-dimensional space) for different source shapes. A single depth estimate for an anomaly is determined where solutions with small errors (determined by the individual algorithms) are clustered. The advantage of this method is the use of multiple algorithms, which increases the confidence of the result. The disadvantages arise from its application to profiles, which limit the data coverage and require that the profiles be orthogonal to the anomaly gradients for accuracy (Blakely, 1995).

Depths estimated by use of aeromagnetic data commonly contain appreciable error that is hard to quantify, because assumptions must be made about the shapes of buried sources (Blakely, 1995). Neither approach used in this study can resolve depths closer than one grid interval (50 m), which was chosen to represent the resolution of the overall survey (Reid, 1980).

Regional Gravity Features

Isostatic residual gravity data indicate that the Española Basin, the northern Albuquerque Basin, and the intervening Santo Domingo Basin form discrete depressions within the central Rio Grande rift (fig. D1). The Santo Domingo Basin is discussed below. The Española Basin is expressed by two northeast-southwest elongated lows contained within a wider, moderate, gravity low (fig. D1). Geophysical models indicate that the eastern elongated low (Velarde graben (VG) and the northern half of the western low (El Alto graben, EA) represent a series of aligned depressions or axial troughs contained within a generally shallow basin (Cordell, 1979; Biehler and others, 1991; Ferguson and others, 1995). The deepest part of the basin (>3 km) is located within the Velarde graben just north of Saint Peters Dome (Cordell, 1979), where it is buried beneath Jemez volcanic rocks that make up the Pajarito plateau (fig. D3). The Velarde graben appears disconnected from the deepest parts of the Santo Domingo Basin, as expressed by gravity lows (fig. D1) and the bedrock elevation model (fig. D4).

The northern Albuquerque Basin is generally bounded by north- and northwest-striking fault systems (Grauch, Gillespie, and Keller, 1999), orientations that differ markedly from the northeast elongations of the Española and Santo Domingo Basins (fig. D1). It is separated from the Santo Domingo Basin by a north-trending gravity high that corresponds with the Ziana horst (ZH, fig. D1), a basement high evident in drill-hole and seismic data (Russell and Snelson, 1994). A 10-km-wide connection between Santa Fe Group sediments of the Santo Domingo Basin and the northern Albuquerque Basin is evident within a northeast-trending trough about 1.5 km deep at the southwestern side of the Santo Domingo Basin (figs. D3, D4).

Santo Domingo Basin

The Santo Domingo Basin corresponds with a large, northeast-elongated gravity low that ranges from 20 to 35 km wide (fig. D1). Basalts of the Santa Ana Mesa volcanic field are located over the deepest part of the gravity low (fig. D1) and the area of thickest (>3 km) basin fill (SAMVF, fig. D3). Major faults are also symmetrically arranged about this area (chapter E, this volume; fig. A3).

The gravity low is bounded on the west by the north-trending gravity high corresponding with the Ziana horst (ZH, fig. D1). The east side of the horst is delineated by the traces of the exposed Tamaya (TM) and Santa Ana (SA) faults (pl. 3, fig. A3). A strong gradient generally follows the Santa Ana fault on the north but diverges from the Tamaya fault on the south.

The northern side of the gravity low consists of a broad gradient that trends northeast from the northern end of the Ziana horst to the southeast corner of Saint Peters Dome (fig. D1). The broadness suggests that this side of the basin is a southeast-dipping homocline or that it is composed of many small faulted steps rather than a few faults with large throw. Mapped faults with good exposure cross the gravity gradient obliquely (MC, BR, CA, SI, and CC, fig. A3). This side of the basin may have originated as an earlier, now inactive and buried, northeast-striking fault system associated with an early, late Miocene to early Pliocene, episode of subsidence in the Santo Domingo Basin (chapter E, this volume).

The southern side of the gravity low trends northeast, following U.S. Interstate 25 from the northwest shoulder of the Sandia Mountains to about 6 km southeast of the La Bajada fault (LB, pl. 3 and fig. A3). Northeast-trending gradient lines along this side of the basin (fig. D1) indicate steeply dipping faults that parallel mapped faults (pl. 3, fig. A3) (Connell and Wells, 1999; Connell, 2002; chapter E, this volume). The steepness of the gravity gradient along most of the southern margin of the basin indicates that, regionally, the faults produce a large, nearly vertical offset. In contrast, the gentler gravity gradients surrounding the Hagan embayment (HEB, fig. D1), especially on the southwest side, suggest a homocline or series of down-to-basin faults.

The eastern side of the Santo Domingo gravity low trends north-northeast from the Hagan embayment to the Santa Fe River (pl. 3, fig. D1). North of the river, the gravity gradient broadens appreciably and gravity gradient lines are oriented in three directions (pl. 3, fig. D1): one that trends northeast-southwest and passes just south of audiomagnetotelluric station 4, one that trends north-south near long 106°15′N., and one that trends north-northwest for a short distance near audiomagnetotelluric station 3. According to the bedrock elevation model (fig. D4), the north-south gradient line is associated with a relatively abrupt, 750-m westward increase in the thickness of basin fill, which marks the eastern margin of the Hagan bench and the western boundary of the Cerrillos uplift.

Cerros del Rio Volcanic Field and Cerrillos Uplift

The gravity high associated with the Cerrillos uplift (Kelley, 1952) is a north-south-elongated high located between the Hagan and Santa Fe embayments (HEB and SE, fig. D1). It includes Eocene and Oligocene intrusions in the Ortiz Mountains and Cerrillos Hills, the lateral extent of which is defined by their magnetic expression (magenta outlines near CH and

OM, fig. D1). The gravity expression and geologic relations (chapter A, this volume) suggest that the uplift is a basement-cored structural uplift rather than a dome caused by intrusion of a laccolith (Stearns, 1953; Disbrow and Stoll, 1957; Grant, 1999). Both the geometry and magnitude of the gravity high are analogous to those associated with other north-south-trending rift-flank uplifts along the margin of the Rio Grande rift, such as the Sangre de Cristo and Sandia Mountains on the eastern sides of the Española and Albuquerque Basins, respectively (fig. D1). The Cerrillos gravity high is arranged en echelon with respect to the similarly oriented gravity high associated with the Sandia Mountains (fig. D1), suggesting a tectonic relation.

The northern termination of the Cerrillos uplift is not well resolved. Basin fill thickens gradually to the north and northeast on this side under cover of the Cerros del Rio volcanic field (CDRVF, fig. D3). Ground-based audiomagnetotelluric soundings suggest that the apparent northward dip of the uplift is accommodated at least in part by a fault between stations 4 and 5 (fig. D1), which offsets the Mancos Shale 600 m down to the north (chapter F, this volume). A northeast-trending gravity gradient line passing just south of audiomagnetotelluric station 4 (fig. D1) is south of the fault inferred from the audiomagnetotelluric data, is not represented by a difference in thickness of basin fill (fig. D3), and does not correspond with any obvious magnetic lineament (fig. D5). These relations suggest that the gravity gradient line represents a pre-rift fault, such as one that juxtaposes basement against pre-Tertiary sedimentary rocks as depicted on cross section E-E′ of plate 6.

Jemez Volcanic Field and Saint Peters Dome

A ridge of moderately high gravity values (3–13 mgal) between the Santo Domingo Basin and the Valles caldera trends westerly from Saint Peters Dome almost to the Jemez River (fig. D1). The gravity ridge probably represents a structural ridge on the Precambrian basement. The area is mostly covered by volcanic rocks of the Jemez field (fig. A1), which are unlikely to produce moderate gravity values because of the relatively low densities indicated by models of the Valles caldera (2,350 kg/m^3; Nowell, 1996). On the west side of the gravity ridge, several en echelon northeast-trending gravity gradient lines mark step-like increases in gravity values to the northwest toward the Nacimiento Mountains (fig. D1), where Precambrian rocks are exposed. The step-wise increases in gravity toward exposed Precambrian rocks suggest that the basement steps up toward the Nacimiento Mountains. A step-faulted basement is evident locally near the Jemez fault zone (JZ, figs. A2, A3), which is near the middle of the three gravity gradient lines (fig. D1). The Jemez fault zone consists of multiple east-northeast- and northeast-striking normal faults, which mostly displace Precambrian and younger rocks down to the east (Goff and others, 1988; Kelley and others, 2003). Cross sections constructed from drill holes show multiple normal faults with cumulative displacements on the Precambrian surface of 470 m down to the south between PC–1 and AET–4 and 254 m down to the southeast between PC–1 and VC–1 (fig. D1; Goff and others, 1988). By inference, basement likely steps down from the Jemez fault area to produce the Saint Peters Dome gravity ridge. Profile modeling, discussed in the section Profile Model Across the La Bajada Constriction, suggests that the Precambrian surface south of Saint Peters Dome is nearly at sea level (~2 km depth). This basement elevation, which is ~1,400 m lower than the Precambrian surface at deep well AET–4 (fig. D1; Goff and others, 1988), may represent a high point of the basement ridge because gravity values are highest in the eastern part of the gravity ridge.

Northeast Santo Domingo Basin and La Bajada Constriction

The northern parts of the San Francisco and Sile faults (SF and SI, figs. A2, A3) divides the Santo Domingo Basin into two principal parts: the deep Santo Domingo Basin beneath Santa Ana Mesa and a shallower bench between the San Francisco and La Bajada fault systems (fig. D4). The area of the bench, where the basin fill averages about 1 km thick (fig. D3), generally corresponds with the Hagan bench of Kelley (1977).

The bedrock elevation model shows a trough that is 10- to 14-km wide and trends northeast where the Rio Grande traverses the Cerros del Rio volcanic field (fig. D4). Santa Fe Group sediments and basalts of the Cerros del Rio field collectively are about 1.25 km thick in the trough (fig. D3). Given that time-domain electromagnetic (TDEM) data indicate the Cerros del Rio basalts are 200–300 m thick (fig. F14*A*), we estimate that sediments within the trough are generally 1 km thick. The relative uniformity of the trough between the Española and Santo Domingo Basins in the thickness and bedrock elevation models (figs. D3, D4) suggests that there may be substantial continuity of basin-fill sediments and facies between the two basins.

Regional Aeromagnetic Features

The principal features of the regional aeromagnetic map (pl. 4, fig. D5) are related to igneous rocks, crystalline basement rocks, magnetic sediments, faults, and anthropogenic structures. We discuss these features in order of prominence on the aeromagnetic map.

A strong negative anomaly that corresponds with the Valles caldera along the northern part of the study area (fig. D5) is likely caused by intracaldera Bandelier Tuff. Ash-flow tuffs erupted during two episodes of caldera collapse (1.61 and 1.22 Ma) are recognized as members of the Bandelier Tuff (Gardner and Goff, 1996). They both likely acquired reversed polarities because they cooled during the latter part of the Matuyama magnetic polarity epoch, when the Earth's field was reversed (fig. C5) (Berggren and others, 1995). Paleomagnetic measurements confirm the reversed polarity (Doell and others,

1968). Although the strong negative anomaly corresponding with the Valles caldera indicates high remanence, outflow sheets of Bandelier Tuff produce very weak magnetic anomalies in the Española Basin (Grauch and Bankey, 2003). Thus, Bandelier Tuff is unlikely to be the cause of the strong negative anomalies located outside the caldera west of Saint Peters Dome and adjacent to the northern part of the Cerros del Rio volcanic field. The anomalies are too poorly resolved in the present data set to identify an alternative possibility.

Basalts of the Santa Ana Mesa volcanic field correspond with many small, mostly negative, high-amplitude anomalies that indicate rocks with strong, reversed-polarity remanence (pl. 4, fig. D5). The 2.5-Ma age of the basalts (Kelley and Kudo, 1978; Smith and Kuhle, 1998b) indicates that they erupted during the early part of the Matuyama epoch (fig. C5). Two strongly negative, north-trending, magnetic anomalies on the east and west sides of the field are associated with two principal chains of volcanic vents (Kelley and Kudo, 1978). A strong negative ellipsoidal anomaly occurs just northwest of the exposed field (fig. D5) in an area mostly covered by young piedmont gravels (Chamberlain and others, 1999). The steep gradients of the anomaly, its similarity to the anomalies associated with vents on Santa Ana Mesa, and limited exposures of basalts (Chamberlain and others, 1999) imply that the source of the anomaly is an isolated, buried volcano that is related to the field.

A distinctive pattern of small anomalies, similar to the pattern over Santa Ana Mesa, is associated with the Cerros del Rio volcanic field (pl. 4, fig. D5). This pattern is composed of positive anomalies as well as mostly negative anomalies. The area is discussed in more detail in the section on the Cochiti Pueblo area.

The broad, high-amplitude, positive elliptical anomaly associated with the Cerrillos Hills (fig. D5) encompasses several outcrops of Eocene and Oligocene monzonite intrusions (unit Tmi, pl. 2), indicating that these intrusions form a composite stock. On the basis of the laccolithic characteristics of these intrusions (Disbrow and Stoll, 1957; Giles, 1995), the stock is likely composed of several overlapping cupola intrusions. The Ortiz Mountains are associated with a similar-looking magnetic high, which also delineates the main lateral extent of a stock. Both of the magnetically defined Cerrillos Hills and Ortiz Mountains stocks (CH and OM, fig. D1) have a more limited areal extent than the gravity high of the Cerrillos uplift that encompasses them. The limited extents of the magnetic anomalies and their clear separation from each other are further evidence that the gravity high is caused by a structural uplift that is more extensive than the two separate stocks.

Prominent, broad, high-amplitude anomalies are associated with the Sandia and Nacimiento Mountains in the south-central and northwestern parts of the study area, respectively (fig. D5). These anomalies reflect uplifted Precambrian crystalline basement that has high total magnetization. A similar, but more subdued, magnetic high lies east of the Cerros del Rio volcanic field, within an area of mapped deposits of the Santa Fe Group in the Española Basin (fig. D5). The source of this anomaly has been interpreted as Precambrian basement buried about 1–2 km below the surface (Grauch and Bankey, 2003).

Sharp linear or curvilinear anomalies are apparent in the high-resolution aeromagnetic data where magnetic relief is low (pl. 4, fig. D5). Many of these anomalies correspond with mapped faults (Grauch, Hudson, and Minor, 2001; Grauch and Bankey, 2003). The aeromagnetic data reveal the full extent of the faults where they are concealed beneath surficial deposits and allow a more comprehensive view of the fault patterns. Many of the major faults have prominent expression in the aeromagnetic data. Examples are the Tamaya (TM) and Santa Ana (SA) faults along the northwestern and western sides of the Santa Ana Mesa volcanic field, the San Francisco fault (SF) in the central part of the study area, and the La Bajada fault zone (LB) (pl. 4, fig. D5). The San Francisco fault, which in the gravity data marks the division between the deep Santo Domingo Basin and the Hagan bench, truncates a strong positive linear anomaly that is associated with the volcaniclastic Espinaso Formation exposed at Espinaso Ridge (pl. 4; ER, fig. D5). The linear anomaly is truncated on the north by faults recognized by Kelley (1977), which we call the Hagan Embayment fault zone (HE, fig. D5). The Espinaso Formation also produces mottled aeromagnetic patterns where it is exposed along the west side of La Bajada fault zone and throughout the Santa Fe embayment (pl. 4; SE, fig. D5) (Grauch and Bankey, 2003).

Not all curvilinear or linear anomalies are related to faults. Linear anomalies between Cerros del Rio volcanic field and Santa Ana Mesa are due to topographic ridges composed of basin-fill deposits of the Cochiti Formation (unit QTc, pls. 2, 5). The common correlation of aeromagnetic data with topography in this area indicates that the Cochiti Formation is fairly magnetic, possibly owing to abundant coarse volcanic clasts derived from the Jemez Mountains (Bailey, Smith, and Ross, 1969; Smith and Lavine, 1996; Smith, McIntosh, and Kuhle, 2001). Coarse-grained facies of the Santa Fe Group correspond with higher magnetization in the northern Albuquerque Basin (Hudson and others, 1999). Similarly, correlation of aeromagnetic anomalies with a series of low bluffs along the east side of the Rio Grande, east of Santa Ana Mesa, indicates that Pleistocene ancient Rio Grande gravel deposits composing the bluffs are fairly magnetic (included in unit QTsa, pl. 5; "magnetic bluffs," fig. D5).

The linear anomaly that trends northwest, subparallel to the Jemez River, from the southern tip of Santa Ana Mesa to the western border of the study area is produced by a cathodically protected pipeline. Very small, isolated, moderate-amplitude positive anomalies, which commonly look like pock marks, are scattered across the aeromagnetic map (pl. 4, fig. D5). These anomalies correspond with anthropogenic features such as landfills, commercial buildings, water tanks, and bridges.

Profile Model Across the La Bajada Constriction

We constructed a two-dimensional model (fig. D6) to fit gravity and magnetic data along a regional profile across the La Bajada constriction (shown on figs. D3–D5 and labeled F-F′ on pl. 2). The profile model provides a general concept of the deep geometry of the La Bajada constriction and neighboring border terranes, which was used to construct the base of the geologic cross section F-F″ (pl. 6). The profile was chosen to cross perpendicular to the northeast-trending trough in the La Bajada constriction (figs. D3, D4), while optimizing its proximity to sources of data, such as gravity stations, wells, and magnetotelluric or audiomagnetotelluric stations (pl. 2). As a consequence, the model cannot fully address many other important features, such as the La Bajada fault zone, because the profile crosses such features obliquely. Gravity data along the profile primarily address the configuration of the basin, whereas magnetic data provide general information on the contacts of the Cerrillos intrusion. In addition, the regional extent of the profile can lead only to general conclusions about the La Bajada constriction, such as major structural blocks and thickness of basin fill.

Knowledge of the physical properties of geologic units involved in the modeling, independent information on their thicknesses and depths, and guides from geologic concepts all are critical for constraining the ambiguities inherent in gravity and magnetic models. The density-depth functions that were developed for the basin-fill thickness and bedrock elevation models (fig. D2) provide reasonable assumptions for densities of the units in the model. Magnetic susceptibilities of the igneous rocks were assigned values that seemed reasonable on the basis of geophysical models for the Española Basin (Grauch and Bankey, 2003). Independent depth constraints come from wells discussed in chapter G (this volume), audiomagnetotelluric and magnetotelluric models described in chapter F (this volume), and concepts developed from geologic studies that are reported elsewhere in this report (primarily chapters A, C, E, and G, this volume) and those by others (Goff, Gardner, and Valentine, 1990; Cather, 1992, 2004; Smith, McIntosh, and Kuhle, 2001; Maynard and Lisenbee, 2002). In addition, a preliminary view of proprietary seismic reflection data (Baldridge and others, 2001) provided conceptual guides just west of the La Bajada fault zone. Note that depth information from the wells and audiomagnetotelluric stations is limited to the top 0.5–1 km, or less than 25 percent of the vertical extent of the model (fig. D6). Individual units that are 100–200 m thick have negligible effect on the fit of the model; for simplicity they are not included in the model. Some geologic units could not be distinguished by physical property (notably the Mesozoic and lower Tertiary rocks); they were modeled as one unit. More detailed discussion of how the independent information was applied and which parts of the model are well or poorly constrained are keyed by number on the profile model (fig. D6) to explanatory notes in table D1.

As in the models of basin-fill thickness and corresponding bedrock elevation (figs. D3, D4), the profile model shows the La Bajada constriction as an asymmetric rift-basin filled with 500 to 1,500 m of Santa Fe Group sediments and Miocene and younger volcanic and volcaniclastic rocks (fig. D6). The deepest part of the basin lies adjacent to the western border terrane, the Saint Peters Dome block. Underlying the rift basin, the profile model is thought to accommodate 1,000–1,300 m of combined thickness of Mesozoic and lower Tertiary rocks, primarily on the basis of geologic considerations (chapter G, this volume).

The western border terrane at Saint Peters Dome consists of structurally elevated Precambrian basement, consistent with interpretations of the regional gravity map discussed in the section Regional Gravity Features. Geologic relations are the primary constraint on the depiction of the sedimentary units overlying the Precambrian basement, where the model shows a poor fit to the gravity data (note 1, fig. D6 and table D1). The gravity data suggest that these units are thinner than expected, that some of the rock units or the basement have a greater density than expected, or a combination of these possibilities.

Over the Cerrillos uplift, the model is consistent with a basement uplift containing the Cerrillos intrusions (fig. D6). The shallow portion of the model is primarily determined from geologic relations (chapter G, this volume; pl. 6*F*). An intrusion of probable Oligocene age beneath Cañada de Santa Fe is indicated in local areas by aeromagnetic and geologic evidence, although it appears to have physical properties that differ from those of the other Cerrillos intrusions (note 6, table D1). Differences in magnetic susceptibilities are required for a model fit of Cerrillos intrusions farther southeast to the observed data (note 9, table D1), which is consistent with a composite stock complex. The nearly vertical boundaries between the differing magnetic susceptibilities on the eastern side of the intrusive complex, which are also required by the model, suggest that laccolithic sills in this area (Stearns, 1953; Disbrow and Stoll, 1957; Grant, 1999) are volumetrically minor compared with the total volume of intrusive material. Grauch and Bankey (2003) reached a similar conclusion from a study of aeromagnetic and gravity data that included the eastern portion of the Cerrillos intrusive complex.

Aeromagnetic Investigations of the Cochiti Pueblo Area

High-resolution aeromagnetic data over the Cochiti Pueblo area (fig. A4) allow us to develop more local aeromagnetic interpretations that are compatible with interpretations of the airborne TDEM data (chapter F, this volume) and the new geologic map compilation (chapters A–E, this volume; pl. 2). Figure D7 displays a color image of the aeromagnetic data within the same geographic area as plate 5 (box on fig. D5). On plate 5, the same aeromagnetic color image is overlain by geologic contacts from the generalized geologic map shown in

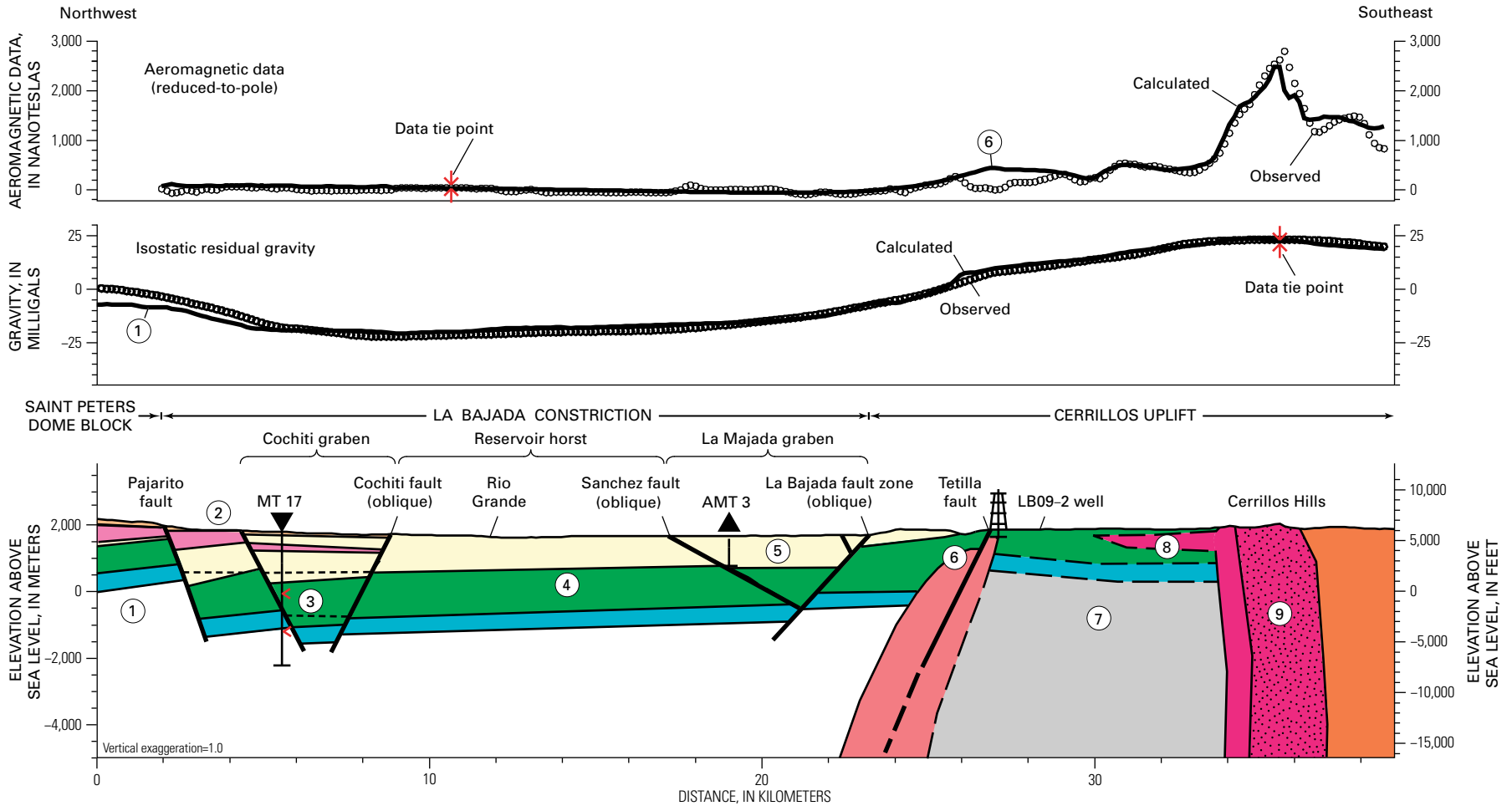

EXPLANATION

Bandelier Tuff
Density, 2,350 kg/m³; susceptibility, 0.01 SI units

Keres Group volcanic rocks
Density, 2,450 kg/m³; susceptibility, 0.01 SI units

Rift-fill sediments and interlayered basalts
Density, 2,170 kg/m³ above and 2,300 kg/m³ below 1.25 km (4,100 ft) depth, respectively

Cerrillos intrusions
Density, 2,710 kg/m³; susceptibility, 0.10 SI units
Density, 2,710 kg/m³; susceptibility, 0.06 SI units
Density, 2,670 kg/m³; susceptibility, 0.07 SI units
Density, 2,570 kg/m³; susceptibility, 0.01 SI units

Lower Tertiary and Mesozoic sedimentary rocks, undifferentiated
Density, 2,400 kg/m³ above and 2,530 kg/m³; below 2.5 km (8,200 ft) depth, respectively

Paleozoic sedimentary rocks
Density, 2,620 kg/m³

Precambrian basement rocks
Density, 2,670 kg/m³; susceptibility, 0
Density, 2,740 kg/m³; susceptibility, 0.03 SI units - see note (7)

Other features
Fault from geologic cross-section (pl. 6*F*)
Boundary constrained by modeling, independent information, or both—Dashed where approximate
Density-depth function boundary
AMT 3 — Audiomagnetotelluric station
MT 17 — Magnetotelluric station
(8) Note explained in table D1

Figure D6 (facing page). Geophysical model of the regional profile oriented northwest-southeast across the La Bajada constriction, coincident with geologic cross section F-F′ (pl. 6*F*; see pl. 2 for line of cross section) or F-F″ (chapter G, this volume). Calculated gravity and magnetic values from model are compared to the corresponding observed isostatic residual gravity and reduced-to-pole aeromagnetic data (pls. 3, 4, respectively). Modeled geologic units and their assigned density in kilograms per cubic meter (kg/m^3) and magnetic susceptibility in SI units are coded by color in explanation. See table D1 for discussion of numbered notes. Magnetic data adjusted by a constant value of 400 nT.

figure C2 and underlain by a shaded digital elevation model. Aeromagnetic anomalies labeled on figure D7 are discussed in the text and provide a key for looking at the same anomalies on plate 5 in comparison with the geology and topography.

Faults were interpreted from the aeromagnetic data following the criteria outlined in the section Locating Faults From Aeromagnetic Data. All interpreted faults are marked on figure D7, but only those that were verified from geologic considerations are incorporated onto plate 2 and discussed in chapter E (this volume). Faults are difficult to detect in the color image of aeromagnetic data (pl. 5, fig. D7). They are best viewed using a shaded-relief display, as in figure D5.

Determining the aeromagnetic expression of exposed igneous rocks in the Cerros del Rio volcanic field places constraints on the nature and age of the buried volcanic rocks elsewhere. Aeromagnetic expression of exposed volcanic units is determined through comparisons of aeromagnetic data, topography, and geology (pls. 2, 5). Many aeromagnetic anomalies have shapes that correspond with topographic features (pl. 5). Examination of these correlations can provide information on the magnetic properties of the rocks composing the terrain (Grauch, 1987). Positive aeromagnetic anomalies that increase in value with increasing relief (positive terrain correlation) indicate a strong induced component, strong normal-polarity remanent component, or both. Negative aeromagnetic anomalies that decrease in value with increasing relief (negative terrain correlation) indicate a strong reversed-polarity remanent magnetization for the rocks that compose the terrain. Preliminary interpretations of polarities from aeromagnetic data for the Tetilla Peak 7.5 minute quadrangle (Sawyer and others, 2001) used magnetic terrain correlations. The interpretations were later generally confirmed by the reconnaissance paleomagnetic study of this report (chapter C, this volume) and are presented in the next section.

Cerros del Rio Volcanic Field

Basalts and andesites of the Cerros del Rio volcanic field possess both reversed and normal remanent magnetic polarities, which are supported by paleomagnetic measurements (chapter C, this volume) and strong positive and negative aeromagnetic anomalies (pl. 5, fig. D7). On the basis of $^{40}Ar/^{39}Ar$ ages, the dual polarities primarily arise from magmatic activity that spanned the transition from the Gauss normal to the Matuyama reversed magnetic polarity epochs at 2.59 Ma (figs. C5, D8). Expression of these polarities in the aeromagnetic data are demonstrated for several mapped volcanic units by comparing the mapped contacts, age data, magnetic terrain correlations, and paleomagnetic measurements (fig. D8). In particular, the relation between positive aeromagnetic anomalies and evidence for normal polarity suggests that moderate- to high-amplitude positive anomalies arise from a dominant normal-polarity remanent magnetization, rather than from a dominant induced magnetization. Negative terrain correlation with Quaternary units likely reflect formation during the latter part of the Matuyama magnetic polarity epoch, coinciding with reverse polarity intervals between 1770 and 1211 ka or 1201 and 1070 ka (fig. C5) (Berggren and others, 1995). An example is the andesite at Cochiti Cone (feature E10, fig. D7; corresponds with unit Qcc, pl. 5).

The relations depicted in figure D8 suggest that the aeromagnetic character of mapped units can be used to help resolve stratigraphic and age relations in the absence of absolute age data (chapter C, this volume), but so doing is beyond the scope of this report. The following general conclusions aid our understanding of buried magnetic sources in the Cochiti Pueblo area.

1. The oldest volcanic units in the field (2.70–2.59 Ma) formed during the Gauss normal magnetic polarity epoch, generally have normal polarity, and are commonly associated with positive aeromagnetic anomalies.

2. Younger volcanic units, Pliocene to Pleistocene in age (2.59 Ma–780 ka), formed during the Matuyama reversed magnetic polarity epoch, generally have reversed polarity, and commonly are associated with negative aeromagnetic anomalies.

Using these relations, we infer that buried basalt of Matuyama age is located in several areas of the volcanic field where strong negative anomalies have no obvious geologic or topographic correlation. One area is north of Tetilla Peak (TP, pl. 1) in the west-central part of the Cerros del Rio field (feature E9, pl. 5 and fig. D7), which is covered by thin Quaternary sheetwash deposits (unit Qsw/Tbt, pl. 5). The source of the negative anomalies is probably buried basalt of Tetilla Hole (unit Tbt), on the basis of samples of this unit in the nearby canyon that give an age of 2.49 Ma (pl. 2) and show reversed polarity (paleomagnetic sample 2MRG–4, pl. 5). An area of negative anomalies in the southwestern part of the field has an elongate shape that is reminiscent of a channel, roughly parallel to the present Cañada de Santa Fe (feature E4, fig. D7). Quaternary sheetwash deposits overlie relatively flat terrain across the area (unit Qsw/Tbr, pl. 5). It may be an old channel, filled with a thickened sequence of reversed-polarity basalt of Caja del Rio (unit Tbr), which is mapped nearby and possesses reversed-polarity remanence (paleomagnetic samples 9MRG–3, 9MRG–10, and 9MRG–11, pl. 5; chapter C, this volume).

Table D1. Explanatory notes keyed to figure D6, Geophysical model of regional profile oriented northwest-southeast across the La Bajada constriction.

Note on figure D6	Explanation
1	Thicknesses of geologic units above the basement derived from geologic constraints (chapter G; pls. 2, 6*F*). The density of the Keres Group volcanic rocks is roughly estimated to be 2,450 kg/m^3, on the basis of expected densities for a mixture of ashflow tuff and volcaniclastic rocks (Telford and others, 1990). The poor fit to the gravity curve could be rectified by a local increase in density of the Keres Group volcanic rocks or Precambrian basement, but geologic considerations discourage further elevation of the Precambrian basement block.
2	Gravity data indicate that the vertical displacement associated with the Pajarito fault zone is distributed over a wide zone, as suggested by the location of the gravity gradient line just southeast of Saint Peters Dome (pl. 3, fig. D1). Therefore, an intermediate block between Saint Peters Dome and the Cochiti graben is required to fit the gravity curve.
3	Cochiti Formation (upper Santa Fe Group) near station MT–17 extends at least 400 m (1,312 ft) deep within the Dome Road well (fig. G5). Depth of penetration of the model for station MT–17 (chapter F) is shown by the line below the inverted solid triangle. Red arrowheads point to the minimum and maximum range of depths (1,900–3,000 m or 6,234–9,843 ft) for the top of the Paleozoic section, which is interpreted as the boundary between low and moderate resistivities as shown on fig. D6. The interface between the Santa Fe Group and underlying lower Tertiary–Mesozoic section is approximately determined by the gravity modeling (fig. D6; bedrock elevation model, fig. D4).
4	The thickness of the Santa Fe Group generally follows the bedrock elevation model (fig. D4). Thickness of underlying section is based on geologic considerations (chapter G, pl. 6*F*) combined with gravity modeling.
5	The oblique angle of the profile model to the strikes of the La Bajada and Sanchez faults inhibits proper modeling of the configuration of the La Majada graben in two dimensions. More comprehensive geologic and geophysical interpretations for the area depict a graben that is filled with sediments, basalt layers, and landslide material to an unknown depth (section Aeromagnetic Investigations of the Cochiti Pueblo Area, chapter D; chapters E and F; pl. 6*F*).
6	A small magnetic stock is indicated below the Cañada de Santa Fe by a lack of correspondence between aeromagnetic patterns and topography in map view (chapter D; anomaly E3 on fig. D7). East of the fault zone, monzonite found at 200 m (656 ft) depth in the LB09–2 well (pl. 6*D*) and exposed in outcrop nearby (pl. 2) argues for a related intrusion at shallower depths, as shown. However, the model requires lower magnetic susceptibility (0.01 SI) and lower density (2,570 kg/m^3) than those for the other Cerrillos intrusions (0.06–0.10 SI and 2,670–2,710 kg/m^3) to fit the gravity and magnetic curves. Altered minerals in the outcrop suggest that the physical properties of the intrusion were modified after emplacement. In addition, the mismatch between the computed magnetic anomaly and the observed data (note 6 along the aeromagnetic curve) coinciding with the eastern half of the intrusion could arise from interference by negative anomalies produced by near-surface reversed-polarity volcanic rocks (fig. D7).
7, 8	Geologic relations at the surface (chapter E; pl. 2) indicate that Upper Cretaceous and older sedimentary units overlying the basement are dipping eastward from the Tetilla fault zone under the volcanic cover of the Cerros del Rio volcanic field. These rocks were intruded to an unknown extent by laccolithic sills related to one of the Cerrillos intrusions (Maynard and Lisenbee, 2002) and by feeder dikes related to the Cerros del Rio basalts (chapter C). The geophysical model cannot adequately represent this geologic complexity. To compensate, we assume a higher magnetic susceptibility (0.03 SI) and density (2,740 kg/m^3) for the underlying basement rocks (note 7) and an arbitrary thickness of material intended to represent the laccolithic character of the Cerrillos intrusion (note 8). In addition, Cerros del Rio basalts are thin in comparison with the scale of the model (pl. 6*F*). They have little influence on the gravity data but contribute in a major way to the observed aeromagnetic data (section Aeromagnetic Investigations of the Cochiti Pueblo Area, chapter D). Because of their minor contribution to the gravity data and their uncertain magnetic properties, we do not attempt to represent them in the model.
9	Composite stocks of the Cerrillos intrusive complex (Maynard and Lisenbee, 2002) are reflected by variations in modeled density (2,670–2,710 kg/m^3) and magnetic susceptibility (0.06–0.10 SI) that are required for a model fit. Even greater variability in the physical properties of the Cerrillos intrusions is likely, which is reflected by the variable match of the computed and observed curves. Although measured values are not available for comparison, the high susceptibilities required by the magnetic modeling indicate that remanence is a major contributor to the total magnetization. Fits to the magnetic curve also indicate that the intrusive contacts are steep at depth.

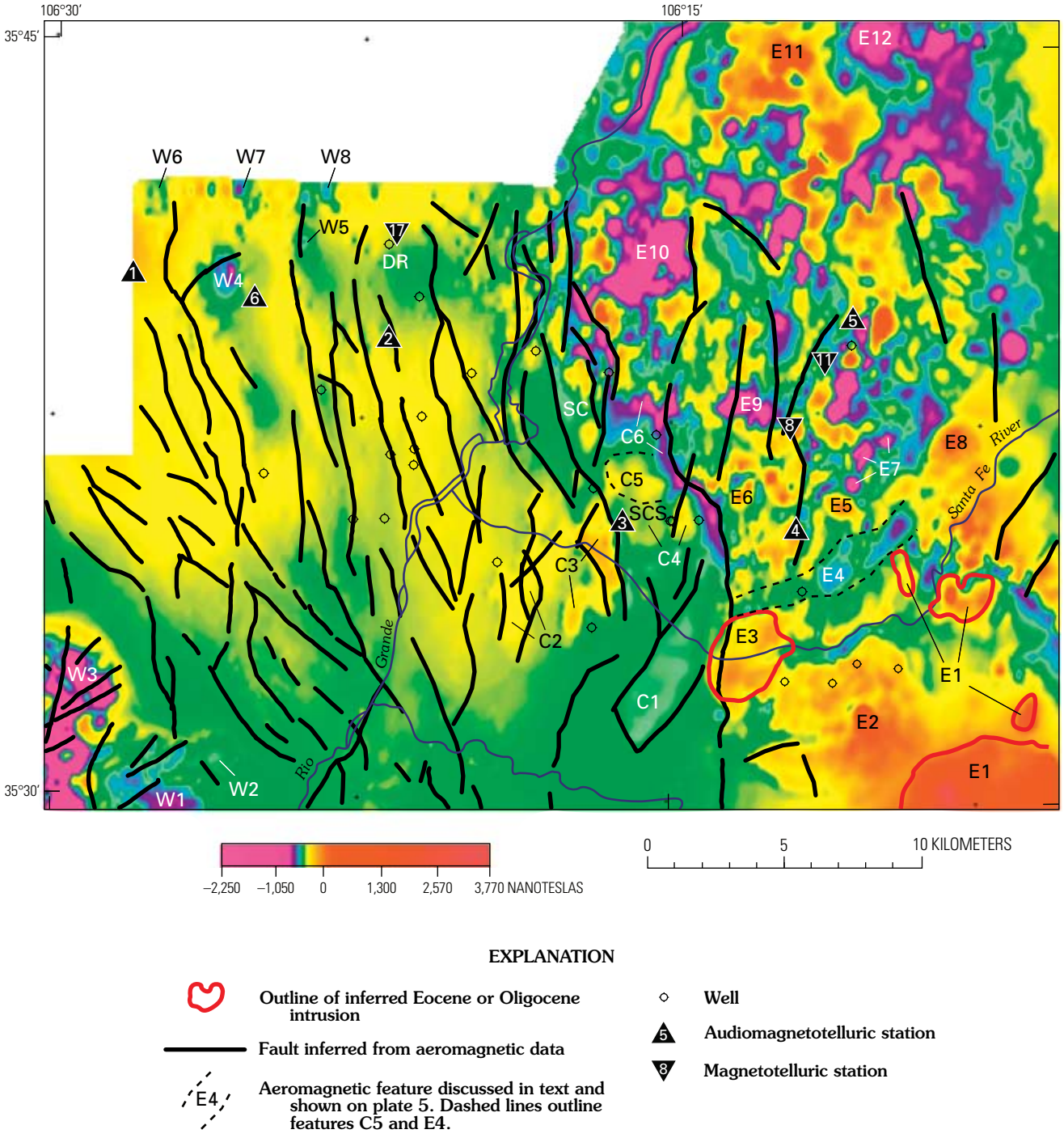

Figure D7. Reduced-to-pole detailed aeromagnetic survey data of Cochiti Pueblo area, shown with color. Interpreted features labeled as discussed in text and referenced in figure D8. Aeromagnetic data are from Sweeney, Grauch, and Phillips (2002). DR, Dome Road well; SC, Sanchez fault; SCS, Santa Cruz Springs Tract well.

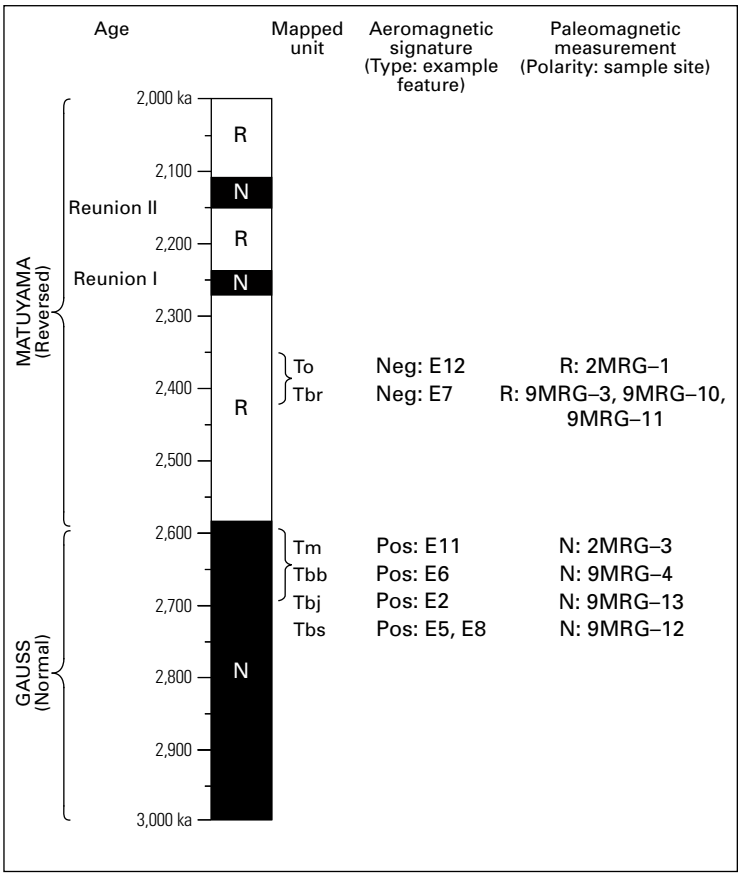

EXPLANATION

Map units (pls. 2, 5)

- To **Andesite of Ortiz Mountain**
- Tbr **Basalt of Caja del Rio**
- Tm **Basaltic andesite of Cerro Montoso**
- Tbb **Basalt of La Bajada**
- Tbj **Basalt of Mesita de Juana**
- Tbs **Basalt of Tsinat Mesa**

Aeromagnetic signature

- Pos: **Positive correlation with terrain**
- Neg: **Negative correlation with terrain**

Letter-number codes refer to anomalies on figure D7

Paleomagnetic measurement

- R: **measured reverse-polarity remanence**
- N: **measured normal-polarity remanence**

Numbers refer to sample sites (pls. 2, 5)

Figure D8. Correspondence between age, magnetic-polarity epoch, aeromagnetic signature, and measured paleomagnetic polarities of some mapped upper Cenozoic volcanic units of the Cerros del Rio volcanic field. Aeromagnetic signature based on correlation of anomalies with terrain in the area of a mapped geologic unit. A positive aeromagnetic signature refers to positive anomalies that correlate in shape and value with the shape and relief of topography. A negative aeromagnetic signature refers to negative anomalies that correlate in shape but inversely in value with relief. Shaded and unshaded columns to right of age scale refer to normal- and reverse-polarity epochs, respectively. Magnetic polarity time scale from Berggren and others (1995) and Honey, Hudson, and Obradovich (1998).

The large, high-amplitude, positive magnetic anomaly associated with the monzonite at the Cerrillos Hills stock complex (fig. D5) and several outlying anomalies related to outcrops of monzonite (unit Tmi and feature E1, pl. 5; feature E1, fig. D7) are evident in the southeastern corner of the aeromagnetic map. A positive anomaly in the western part of Cañada de Santa Fe (feature E3, fig. D7) corresponds poorly with terrain even though a deep canyon crosses its northern extent. The lack of correspondence with terrain suggests that the source lies buried below the depth of the canyon bottom. It may be an Oligocene intrusion related to the Cerrillos Hills intrusive rocks (chapter C, this volume). On the other hand, no anomalies are associated with two occurrences of monzonite nearby. One is a small outcrop located about 2 km up-canyon from the feature E3 anomaly (unit Tmi, pl. 2; not shown on pl. 5). The other was found at 200 m depth in well LB09–2 (pl. 6*D*, fig. D6, and discussion in chapter G, this volume), located on the south rim of Cañada de Santa Fe (fig. G1).

Cochiti Graben

Throughout most of the Cochiti graben (figs. A4, E9), the relatively magnetic Cochiti Formation (unit QTc, pl. 5) and axial river gravels (unit QTsa) produce aeromagnetic anomalies with amplitudes of about 20–30 nT (pl. 4, fig. D5). Many of these linear anomalies correlate with terrain (compare pls. 4 and 5), but others have steep gradients that cannot be due solely to terrain. They have been interpreted as faults by following the criteria outlined in the section Locating Faults From Aeromagnetic Data. These and other faults interpreted from the aeromagnetic data (fig. D7) contributed to the overall understanding of faults in the study area (chapter E, this volume).

Several areas in the northwestern part of the study area have negative anomalies that indicate reversed-polarity sources (features W4–W8, pl. 5 and fig. D7.). Although Bandelier Tuff is exposed in the area of two of these anomalies (units Qbt, Qbo, pl. 5; features W7, W8, pl. 5 and fig. D7), its expected low magnetization (discussed previously) suggests that the source is buried underneath the tuff. For two reasons, rocks related to the Bearhead Rhyolite (unit Trb, pl. 2) are the likely source. First, a separate high-amplitude negative anomaly in the area (feature W4) is centered on an exposed lava dome of Bearhead Rhyolite (pl. 5). Second, moderately high resistivities (>200 ohm-m) at depths of 50–200 m (feature W4, fig. F7*B–E*) encompass all the negative anomalies except feature W5. The source under feature W5 is not apparent.

Variations in the amplitude and extent of negative anomalies (features W1–W3, pl. 5 and fig. D7) are evident over reversed-polarity basalts on Santa Ana Mesa (unit Tbk_{1-3}, pl. 5). The variations in amplitude cannot be directly correlated with the extent of mapped units. For example, the most negative values (less than –500 nT at feature W3) generally follow the oldest mapped basalt (unit Tbk_1, pl. 5), but they only partially correspond with a younger basalt (unit Tbk_2, pl. 5) at the northern mesa edge. Anomalies with moderately negative values (–100 to –500 nT at features W1 and W2) extend over mapped basalt to the mesa edge, but they do not differ in character across a mapped contact between two of the units (Tbk_2 and Tbk_3, pl. 5). These relations suggest that the sources lie mostly beneath the surface, consistent with the interpretation that the high-amplitude negative anomalies are related to intrusive material underlying the vents.

Central Reservoir Horst

The central Reservoir horst lies between the Cochiti and Sanchez faults (figs. A4, E9). The Sanchez fault can be traced by using aeromagnetic data from where it is mapped at the Rio Grande to the south along the sides of elongated anomalies or between breaks in anomalies for about 10 km (SC, fig. D7). This magnetic boundary is most apparent in the color shaded-relief display (SC, fig. D5). The fault is also apparent in resistivity cross sections from the TDEM data (chapter F, this volume). The Sanchez fault also bounds the west side of the La Majada graben (figs. A4, E9).

Two adjacent areas of high magnetic values (amplitudes 150–200 nT) appear related (feature C3, pl. 5 and fig. D7). The areas of high magnetic values correspond with an area of moderate (about 100 ohm-m) resistivities apparent in the TDEM depth slices from 100–200 m (fig. F7*D–F*) and in the TDEM cross section for line 630 below 100 m depth at easting 384 km (fig. F11*D*). Magnetotelluric station 3 requires a resistor (100 ohm-m) in this location as well (fig. F5). The correlation of aeromagnetic data and resistivity models and the large vertical extent of the moderate-resistivity values suggest that the source of the aeromagnetic anomalies is a volcanic vent or shallow intrusion. The 2.71-Ma basalt of Peña Blanca (unit Tbpb, pl. 2; not distinguished on pl. 5) may have flowed from the inferred vent. It is exposed about 3 km to the west and dips gently to the east underneath Santa Fe Group sediments toward the inferred vent. Its correspondence with positive aeromagnetic values (feature C2, fig. D7), which suggests a normal-polarity remanence, is compatible with its formation during the normal-polarity Gauss epoch (fig. C5). Another vent and possible source of the Peña Blanca basalt inferred from geologic relations near Cochiti Dam (G.A. Smith, University of New Mexico, oral commun., 1998) is located on the northwest edge of the area of high aeromagnetic values. Its proximity suggests that the vents inferred from geophysical and geological data may be genetically related.

The estimates of minimum depth to the source of anomaly C3, as derived from the gridded RTP data, fall within the range 50–100 m (open circles, pl. 5), which is comparable to the 100-m minimum depth obtained from resistivity models (line 630, fig. F11*D*). In contrast, maximum depth estimates from the pseudogravity grid (× symbols, pl. 5) give values of 100 m on the west compared with 200–250 m on the east. The variation in estimates of minimum and maximum depth implies that the source is thin (sheet-like) on the west and thicker to the east, a configuration that is suggested, but not well resolved, by TDEM data (fig. F11*D*).

La Majada Graben

Within the La Majada graben (figs. A4, E9), two areas of positive magnetic anomalies (features C4 and C5, pl. 5 and fig. D7) have amplitudes on the order of 100 nT. These anomalies correspond with the lateral extents of moderately high resistors in the TDEM inversions: 50–300 ohm-m in feature C4 from 50–100 m depth (fig. F7*B–D*) and 50–125 ohm-m for feature C5 from 70–200 m depth (figs. F7*C–F* and F11*G*, line 626 at easting 385–386 km). Minimum depth estimates from the gridded RTP data (50–100 m, open circles, pl. 5) agree with the resistivity inversions, whereas the maximum depth estimates from the gridded pseudogravity data (250–500 m, H symbols, pl. 5) do not. The large estimates of maximum depth suggest that the magnetic sources are continuous to 250–500 m depth, rather than to more shallow depths as indicated by the TDEM results.

The Santa Cruz Springs Tract well (SCS, fig. D7; fig. G3) may provide an explanation for this discrepancy in the vicinity of feature C4, despite its location within an anomalous area of low magnetic values near an inferred fault (pl. 5, fig. D7). Santa Fe Group sediments in the well are medium to coarse grained and, as compared with deposits higher in the well, contain more volcanic clasts between about 40–100 m depth (fig. G3). Grain size is finer from 100 to 165 m depth. The thickness and depths of coarse material overlying finer material are compatible with the TDEM results down to at least 200 m depth in the vicinity of the well (fig. F7*A–F*). The magnetic properties of the coarse-grained sediments are probably comparable to those of the Cochiti Formation, suggesting that they may be an important contributor to the magnetic anomalies but are not their sole source. Basalt encountered at depths of 165–256 m in the well are dated at 2.59 Ma or older (fig. G3). This age suggests that the rocks have normal-polarity remanence and would produce positive aeromagnetic anomalies (fig. D8). Thus, we suggest that the aeromagnetic anomalies of features C4 and possibly C5 are caused by two separate sources that are considered as one by the depth estimation algorithm. The two sources are coarse-grained Santa Fe Group at a moderate level and basalt of probable Gauss age at deeper levels. The TDEM inversions, which did not penetrate deep enough to detect the basalt, reflect only the variations in the Santa Fe Group.

The strong negative anomaly beside the La Bajada fault (feature C6, pl. 5 and fig. D7) has several possible explanations: (1) Large slump blocks (unit Qlc, pl. 5) that are composed of reversed-polarity basalts and have experienced minor reorientation, (2) reversed-polarity Quaternary flows from Cochiti Cone (chapter C, this volume; feature E10, pl. 5 and fig. D7), (3) effects of the geometry of the magnetic sources at the fault (Grauch, Hudson, and Minor, 2001), (4) magnetic-terrain effects related to the escarpment and the position of the airplane that collected the data, or (5) some combination of these possibilities. The first two possibilities are supported by evidence in the TDEM depth-slice maps of moderately high resistivities that do not extend below 150 m depth (fig. F7). However, the TDEM data in this area are influenced by the large differences in flight elevation across the La Bajada escarpment (chapter F, this volume).

An elongated negative anomaly in the southern part of the La Majada graben (feature C1, pl. 5 and fig. D7) measures about 6–7 km long and 2 km wide, is oriented northeast-southwest, and shows most prominently in the color shaded-relief display (fig. D5). The negative anomaly and shape of the source indicate a reversed-polarity volcanic flow, likely related to one of the volcanic units exposed in the Cerros del Rio volcanic field that erupted after 2.59 Ma (figs. C5, D8). The anomaly edges are fairly linear and abrupt (fig. D5), suggesting that the flow has been faulted or is fault controlled (fig. D7). North of the Santa Fe River, the eastern edge of the anomaly curves into the La Bajada fault zone; to the south it parallels the trace of the southern Tetilla fault zone (pl. 5). Profile-based estimates of depth and source type (described in the section Estimating Depth) were determined for two profiles across the anomaly (red lines, pl. 5). The results indicate the source is thin compared with its width (that is, sheet-like), dips to the east, and lies at 270–340 m depth on the northwestern side and 410–490 m depth on the southeastern side (red ticks along the profiles, pl. 5). For comparison, the range of maximum depths determined from gridded RTP and pseudogravity data is 200–250 m on the northwestern side and 500–700 m on the southeastern side (H symbols, pl. 5). The negative anomaly also has little relation to areas of high resistivity on the TDEM depth slice maps (fig. F7), which is consistent with a source at depths greater than 200–250 m, below the expected detection limit of the TDEM survey in this area (chapter F, this volume).

The buried flow producing the negative anomaly in the southern part of the graben (feature C1, pl. 5 and fig. D7) may be related to the ~2.4 Ma basalt of Caja del Rio (unit Tbr, pl. 5), because this unit has reversed polarity remanence and is exposed nearby, east of the La Bajada fault zone (chapter C, this volume; paleomagnetic sample 9MRG–3, pl. 5). The difference between the estimated 1,150–1,350 m elevation of the buried flow and the ~1,875 m elevation of the exposures of basalt of Caja del Rio on the mesa east of the fault zone is 525–725 m, which gives a rough estimate on the amount of cumulative throw that may have been accommodated by the La Bajada fault zone in the last 2.4 m.y.

Summary

Gravity data for the study area contribute to an overall understanding of basin geometry, the nature and orientation of basement structures, and regional variations in thickness of basin fill. Aeromagnetic data help determine the lateral limits of intrusions, delineate buried faults and igneous rocks and, in some places, clearly distinguish between basalts extruded during different magnetic polarity epochs. Combined with geologic and geophysical constraints provided by the other chapters in this report, gravity and magnetic interpretations contribute directly and indirectly to the subsurface geologic

and hydrogeologic framework model that is presented in chapter G (this volume). The salient interpretations are enumerated as follows.

1. The Santo Domingo Basin is expressed as a large rhombic gravity low, elongated on northeast-trending structures on its northwestern and southeastern sides (fig. D1). The gravity gradients surrounding the low indicate that the basin is bounded by steeply dipping faults of large vertical displacement on the southeastern side and by a homocline or series of down-to-basin faults on the northwestern side. The Hagan bench and the La Bajada constriction occupy the northeastern part of the basin. The Ziana horst and an unnamed trough connecting the Santo Domingo and Albuquerque Basins lie on the southwestern side. Many well-exposed faults along the northwestern side strike north-northwest oblique to the northeast trend of the basin margins (chapter E, this volume; fig. A3).

2. The Cerrillos uplift is reflected in a north-south gravity high that includes and is much larger than the area of Oligocene intrusions of the Ortiz Mountains and Cerrillos Hills, as indicated by the regional magnetic data. This gravity expression is consistent with a basement-cored rift-flank uplift, analogous to the Sandia Mountains. The western boundary follows the southern portion of the La Bajada fault zone, and the eastern boundary corresponds with the western, synclinal limb of the Santa Fe embayment. The northern termination of the Cerrillos uplift is located under the Cerros del Rio volcanic field. A gravity gradient line trending northeast from the mouth of Cañada de Santa Fe is probably due primarily to thickening of pre-Tertiary rocks. Santa Fe Group sediments also thicken farther to the north and northeast.

3. A moderate gravity high that trends westerly from Saint Peters Dome is primarily due to elevated Precambrian basement (approximately 2 km deep) that gradually steps up toward the Nacimiento Mountains, where it is exposed.

4. Within the La Bajada constriction, the gravity data and associated models indicate a northeast-trending trough, 10–14 km wide, that likely contains Santa Fe Group sediments about 1 km thick. The trough projects from the northeastern part of the Santo Domingo Basin just northwest of Cochiti Dam to the southwestern part of the Española Basin about 10 km east of Saint Peters Dome. It is buried under 200–300 m of basalt in the Cerros del Rio volcanic field for most of its extent. A profile model across the constriction emphasizes that the rift basin is somewhat asymmetric in that the deepest part lies adjacent to the Saint Peters Dome block on the west.

5. Comparison of high-resolution aeromagnetic data for the Cerros del Rio volcanic field with topography, age dating, geologic mapping, and paleomagnetic measurements indicates that mapped volcanic units formed during the Gauss normal magnetic-polarity epoch (2.70–2.59 Ma) are associated with moderate- to high-amplitude positive anomalies, whereas those units formed during the Matuyama reversed magnetic-polarity epoch (2.59 Ma–776 ka) are associated with moderate- to high-amplitude negative anomalies. These relations can be used to aid geologic mapping of basalts within the volcanic field and to interpret aeromagnetic anomalies related to buried igneous rocks west of the field.

6. Throughout much of the western half of the Cochiti Pueblo study area, sediments at the surface are magnetic enough to produce aeromagnetic anomalies that correlate with topography. These anomalies are especially apparent over exposures of volcaniclastic deposits of the Cochiti Formation and interfingering axial river gravels. Numerous offsets of these magnetic sediments along faults produce aeromagnetic gradients that appear linear in shaded-relief displays of the data. These aeromagnetic expressions help delineate faults where they are concealed or inferred.

7. The aeromagnetic data help define the southern part of the Sanchez fault, which divides the Reservoir horst on the west from the La Majada graben on the east.

8. An extensive northeast-elongated negative anomaly in the southern part of the La Majada graben is interpreted as a buried, possibly fault-bounded flow that dips to the east and ranges in depth from about 300 to 450 m. The buried flow was probably erupted after 2.59 Ma, possibly related to the ~2.4-Ma basalt of Caja del Rio. These basalts are exposed 525–725 m higher east of the La Bajada fault zone on top of the Caja del Rio Plateau. This elevation difference gives a rough estimate of the amount of throw that may have occurred along the La Bajada fault zone in the last 2.4 m.y.

References Cited

Bailey, R.A., Smith, R.L., and Ross, C.S., 1969, Stratigraphic nomenclature of volcanic rocks in the Jemez Mountains, New Mexico: U.S. Geological Survey Bulletin 1274–P, 19 p.

Baldridge, W.S., Ferguson, J.F., Braile, L.W., Biehler, S., Jiracek, G.R., Gilpin, B.E., Alumbaugh, D.L., Gratwick, D.S., Richards, T.L., and Hasterok, D.P., 2001, Architecture of the southern Espanola Basin (Rio Grande rift) and flank uplift adjacent to the La Bajada fault [abs.]: Geological Society of America Abstracts with Programs, v. 33, no. 5, p. 61.

Bartolino, J.R., and Cole, J.C., 2002, Ground-water resources of the Middle Rio Grande Basin, New Mexico: U.S. Geological Survey Circular 1222, 132 p.

Bath, G.D., 1968, Aeromagnetic anomalies related to remanent magnetism in volcanic rock, Nevada Test Site: Geological Society of America Memoir 110, p. 135–146.

Berggren, W.A., Kent, D.V., Swisher, C.C., III, and Aubry, M.P., 1995, A revised Cenozoic geochronology and chronostratigraphy, *in* Berggren, W.A., Kent, D.V., Aubry, M.P., and Hardenbol, J., eds., Geochronology, time scales and global stratigraphic correlation: SEPM (Society of Sedimentary Geologists) Special Publication 54, p. 129–212.

Biehler, Shawn, Ferguson, J.F., Baldridge, W.S., Jiracek, G.R., Aldern, J.L., Martinez-Garcia, M., Fernandez, R., Romo, J., Gilpin, B., Braile, L.W., Hersey, D.R., Luyendyk, B.P., and Aiken, C.L.V., 1991, A geophysical model of the Española Basin, Rio Grande rift, New Mexico: Geophysics, v. 56, p. 340–353.

Birch, F.S., 1982, Gravity models of the Albuquerque Basin, Rio Grande rift: Geophysics, v. 47, p. 1185–1197.

Blakely, R.J., 1995, Potential theory in gravity and magnetic applications: Cambridge, U.K., Cambridge University Press, 441 p.

Blakely, R.J., and Jachens, R.W., 1991, Regional study of mineral resources in Nevada—Insights from three-dimensional analysis of gravity and magnetic anomalies: Geological Society of America Bulletin, v. 103, p. 795–803.

Butler, R.F., 1992, Paleomagnetism—Magnetic domains to geologic terranes: Boston, Blackwell, 319 p.

Cather, S.M., 1992, Suggested revisions to the Tertiary tectonic history of north-central New Mexico: New Mexico Geological Society 43d field conference, San Juan Basin IV, Guidebook, p. 109–122.

Cather, S.M., 2004, Laramide orogeny in central and northern New Mexico and southern Colorado, *in* Mack, G.H., and Giles, K.A., eds., The geology of New Mexico: New Mexico Geological Society Special Publication 11, p. 203–248.

Chamberlin, R.M., Pazzaglia, F.J., Wegmann, K.W., and Smith, G.A., 1999, Preliminary geologic map of the Loma Creston 7.5 minute quadrangle, Sandoval County, New Mexico, New Mexico Bureau of Mines and Mineral Resources Open-file Geologic Map OF–GM 25, scale 1:24,000.

Connell, S.D., 2002, Geology of the northern Sandia Mountains and Albuquerque Basin, Placitas, and Bernalillo area, Sandoval Country, New Mexico: New Mexico Bureau of Mines and Mineral Resources New Mexico Decision-Makers Field Guide 1, p. 140–143.

Connell, S.D., and Wells, S.G., 1999, Pliocene and Quaternary stratigraphy, soils, and tectonic geomorphology of the northern flank of the Sandia Mountains, New Mexico—Implications for the tectonic evolution of the Albuquerque Basin: New Mexico Geological Society 50th field conference, Albuquerque Basin, Guidebook, p. 379–391.

Cordell, Lindrith, 1976, Aeromagnetic and gravity studies of the Rio Grande graben in New Mexico between Belen and Pilar: New Mexico Geological Society Special Publication 6, p. 62–70.

Cordell, Lindrith, 1979, Gravimetric expression of graben faulting in Santa Fe country and the Española Basin, New Mexico: New Mexico Geological Society 30th field conference, Santa Fe Country, Guidebook, p. 59–64.

Cordell, Lindrith, and Grauch, V.J.S., 1985, Mapping basement magnetization zones from aeromagnetic data in the San Juan Basin, New Mexico, *in* Hinze, William J., ed., The utility of regional gravity and magnetic anomaly maps: Society of Exploration Geophysicists, p. 181–197.

Disbrow, A.E., and Stoll, W.C., 1957, Geology of the Cerrillos area, Santa Fe County, New Mexico: New Mexico Bureau of Mines and Mineral Resources Bulletin 48, 73 p.

Doell, R.R., Dalrymple, G.B., Smith, R.L., and Bailey, R.A., 1968, Paleomagnetism, potassium-argon ages, and geology of rhyolites and associated rocks of the Valles caldera, New Mexico: Geological Society of America Memoir 116, p. 211–248.

Ferguson, J.F., Baldridge, W.S., Braile, L.W., Biehler, S., Gilpin, B., and Jiracek, G.R., 1995, Structure of the Española Basin, Rio Grande rift, from SAGE seismic and gravity data: New Mexico Geological Society 46th field conference, Santa Fe Region, Guidebook, p. 105–110.

Gardner, J.N., and Goff, Fraser, 1996, Geology of the northern Valles caldera and Toledo embayment, New Mexico: New Mexico Geological Society 47th field conference, Jemez Mountains Region, Guidebook, p. 225–230.

Giles, D.L., 1995, Cerrillos mining district: New Mexico Geological Society 46th field conference, Santa Fe Region, Guidebook, p. 61–62.

Gillespie, C.L., Grauch, V.J.S., Oshetski, Kim, and Keller, G.R., 2000, Principal facts for gravity data collected in the southern Albuquerque Basin and a regional compilation, central New Mexico: U.S. Geological Survey Open-File Report 00–490; digital data available from http://pubs.usgs.gov/of/2000/ofr-00-0490/.

Goff, Fraser, Gardner, Jamie, and Valentine, Greg, 1990, Geologic map of the St. Peters Dome area, Jemez Mountains, New Mexico: New Mexico Bureau of Mines and Mineral Resources Geologic Map 69, scale 1:24,000.

Goff, Fraser, Shevenell, Lisa, Gardner, J.N., Vuataz, F.-D., and Grigsby, C.O., 1988, The hydrothermal outflow plume of Valles caldera, New Mexico, and a comparison with other outflow plumes: Journal of Geophysical Research, v. 93, p. 6041–6058.

Grant, P.R., 1999, Subsurface geology and related hydrologic conditions, Santa Fe embayment and contiguous areas, New

Mexico: New Mexico Geological Society 50th field conference, Albuquerque Geology, Guidebook, p. 425–435.

Grauch, V.J.S., 1987, A new variable-magnetization terrain correction method for aeromagnetic data: Geophysics, v. 52, no. 1, p. 94–107.

Grauch, V.J.S., 2001a, Using high-resolution aeromagnetic surveys to map subsurface hydrogeology in sediment-filled basins—A case study over the Rio Grande rift, central New Mexico, USA: Exploration Geophysics, v. 32, p. 209–213.

Grauch, V.J.S., 2001b, High-resolution aeromagnetic data, a new tool for mapping intrabasinal faults—An example from the Albuquerque Basin, New Mexico: Geology, v. 29, p. 367–370.

Grauch, V.J.S., and Bankey, Viki, 2003, Aeromagnetic interpretations for understanding the hydrogeologic framework of the southern Española Basin, New Mexico: U.S. Geological Survey Open-File Report 03–124, available at http://pubs.usgs.gov/of/2003/ofr-03-124/.

Grauch, V.J.S., and Cordell, Lindrith, 1987, Limitations of determining density or magnetic boundaries from the horizontal gradient of gravity or pseudogravity data: Geophysics, v. 52, no. 1, p. 118–121.

Grauch, V.J.S., Gillespie, C.L., and Keller, G.R., 1999, Discussion of new gravity maps for the Albuquerque Basin area: New Mexico Geological Society 50th field conference, Albuquerque Geology, Guidebook, p. 119–124, plates C and D, p. 136–137.

Grauch, V.J.S., Hudson, M.R., and Minor, S.A., 2001, Aeromagnetic expression of faults that offset basin fill, Albuquerque Basin, New Mexico: Geophysics, v. 66, p. 707–720.

Grauch, V.J.S., and Johnston, C.S., 2002, Gradient window method—A simple way to separate regional from local horizontal gradients in gridded potential-field data [abs.]: 2002 Technical Program Expanded Abstracts, 72d Annual Meeting, Society of Exploration Geophysicists, p. 762–765.

Grauch, V.J.S., Rodriguez, B.D., and Deszcz-Pan, Maria, 2002, How geophysical methods have been used to understand the subsurface, *in* Bartolino, J.R., and Cole, J.C., Ground-water resources of the middle Rio Grande Basin, New Mexico: U.S. Geological Survey Circular 1222, p. 36–37.

Hester, D.J., 1998, USGS Middle Rio Grande Basin Study develops terrain data: New Mexico Geographic Information Council, The Map Legend newsletter, spring/summer 1998, v. 9, no. 2, p. 3.

Heywood, C.E., 1992, Isostatic residual gravity anomalies of New Mexico: U.S. Geological Survey Water-Resources Investigations Report 91–4065, 27 p.

Honey, J.G., Hudson, M.R., and Obradovich, J.D., 1998, The occurrence of the Reunion II subchron in lacustrine beds in the Beaver Basin, Utah, *in* Tomida, Y., Flynn, L.J., and Jacobs, L.L., eds., Advances in vertebrate paleontology and geochronology, Tokyo National Science Museum Monograph 14, p. 17–38.

Hudson, M.R., Mikolas, Marlo, Geissman, J.W., and Allen, B.D., 1999, Paleomagnetic and rock magnetic properties of Santa Fe Group sediments in the 98th Street core hole and correlative surface exposures, Albuquerque Basin, New Mexico: New Mexico Geological Society 50th field conference, Albuquerque Basin, Guidebook, p. 355–361.

Jachens, R.C., and Moring, B.C., 1990, Maps of the thickness of Cenozoic deposits and the isostatic residual gravity over basement for Nevada: U.S. Geological Survey Open-File Report 90–404, 15 p.

Kelley, Shari, Kempter, K.A., Goff, Fraser, Rampey, M., Osburn, G.R., and Ferguson, C.A., 2003, Geology of the Jemez Springs 7.5 minute quadrangle, Sandoval County, New Mexico: New Mexico Bureau of Geology and Mineral Resources Open-file Geologic Map OF–GM 73, scale 1:24,000

Kelley, V.C., 1952, Tectonics of the Rio Grande depression of central New Mexico: New Mexico Geological Society 3d field conference, Rio Grande Country, Guidebook, p. 92–105.

Kelley, V.C., 1977, Geology of Albuquerque Basin, New Mexico: New Mexico Bureau of Mines and Mineral Resources Memoir 33, 60 p.

Kelley, V.C., and Kudo, A.M., 1978, Volcanoes and related basalts of Albuquerque Basin, New Mexico: New Mexico Bureau of Mines and Mineral Resources Circular 156, 30 p., 2 plates.

Kucks, R.P., Hill, P.L., and Heywood, C.E., 2001, New Mexico aeromagnetic and gravity maps and data—A web site for distribution of data, version 1.0: U.S. Geological Survey Open-File Report 01–0061, available at http://pubs.usgs.gov/of/2001/ofr-01-0061/.

Maynard, S.R., and Lisenbee, A.L., 2002, Geology of the Picture Rock 7.5 minute quadrangle, Santa Fe County, New Mexico, New Mexico Bureau of Geology and Mineral Resources Open-file Geologic Map OF–GM 51, scale 1:12,000.

Nowell, D.A.G., 1996, Gravity modelling of the Valles caldera: New Mexico Geological Society 47th field conference, Jemez Mountains Region, Guidebook, p. 121–128.

Phillips, J.D., 1997, Potential-field geophysical software for the PC, version 2.2: U.S. Geological Survey Open-File Report 97–725. Available at http://pubs.usgs.gov/of/1997/ofr-97-0725/.

Phillips, J.D., 2000, Locating magnetic contacts—A comparison of the horizontal gradient, analytic signal, and local wavenumber methods [abs.]: 2000 Technical Program Expanded Abstracts, 70th Annual Meeting, Society of Exploration Geophysicists, p. 402–405.

Reid, A.B., 1980, Aeromagnetic survey design: Geophysics, v. 45, no. 5, p. 973–976.

Reynolds, R.L., Rosenbaum, J.G., Hudson, M.R., and Fishman, N.S., 1990, Rock magnetism, the distribution of magnetic minerals in the Earth's crust, and aeromagnetic anomalies: U.S. Geological Survey Bulletin 1924, p. 24–45.

Roest, W.R., and Pilkington, Mark, 1993, Identifying remanent magnetization effects in magnetic data: Geophysics, 58, 653–659.

Russell, L.R., and Snelson, S., 1994, Structure and tectonics of the Albuquerque Basin segment of the Rio Grande rift—Insights from reflection seismic data, *in* Keller, G.R., and Cather, S.M., eds., Basins of the Rio Grande rift—Structure, stratigraphy, and tectonic setting: Geological Society of America Special Paper 291, p. 83–112.

Sawyer, D.A., Shroba, R.R., Minor, S.A., and Thompson, R.A., 2001, Geologic map of the Tetilla Peak quadrangle, Santa Fe and Sandoval Counties, New Mexico: U.S. Geological Survey Miscellaneous Field Studies Map MF–2352, scale 1:24,000.

Simpson, R.W., Jachens, R.C., Blakely, R.J., and Saltus, R.W., 1986, A new isostatic map of the conterminous U.S. with a discussion on the significance of isostatic residual anomalies: Journal of Geophysical Research, v. 91, p. 8348–8372.

Smith, G.A., and Kuhle, A.J., 1998b, Geologic map of the Santo Domingo Pueblo SW 7.5 minute quadrangle, Sandoval County, New Mexico: New Mexico Bureau of Mines and Mineral Resources Open-file Digital Map OF–DM–26, 1 sheet and text, scale 1:24,000.

Smith, G.A., and Lavine, Alex, 1996, What is the Cochiti Formation?: New Mexico Geological Society 47th field conference, Jemez Mountains Region, Guidebook, p. 219–224.

Smith, G.A., McIntosh, W., and Kuhle, A.J., 2001, Sedimentologic and geomorphic evidence for seesaw subsidence of the Santo Domingo accommodation-zone basin, Rio Grande rift, New Mexico: Geological Society of America Bulletin, v. 113, p. 561–574.

Stearns, C.E., 1953, Tertiary geology of the Galisteo-Tonque area, New Mexico: Geological Society of America Bulletin, v. 64, p. 459–508.

Sweeney, R.E., Grauch, V J.S., and Phillips, J.D., 2002, Merged digital aeromagnetic data for the Albuquerque and southern Española Basins, New Mexico: U.S. Geological Survey Open-File Report 02–205, available at http://pubs.usgs.gov/of/2002/ofr-02-0205/.

Telford, W.M., Geldart, L.P., and Sheriff, R.E., 1990, Applied geophysics (2d ed.): Cambridge, U.K., Cambridge University Press, 770 p.

U.S. Geological Survey, Sander Geophysics, Ltd., and Geoterrex-Dighem, 1999, Digital aeromagnetic data from the Sandoval–Santa Fe, Belen, and Cochiti airborne surveys, covering areas in Rio Arriba, Sandoval, Santa Fe, Socorro, and Valencia Counties, New Mexico: U.S. Geological Survey Open-File Report 99-404, 1 CD–ROM

Published in the Central Region, Denver, Colo.
Manuscript approved for publication February 10, 2006
Graphics by authors
Photocomposition by Mari L. Kauffmann (Contractor, ATA Services)
Edited by Mary-Margaret Coates (Contractor, ATA Services)